Rep. Prog. Phys., Vol. 41, 1978. Printed in Great Britain

Incoherent scatter of radio waves from the ionosphere

W J G BEYNON and P J S WILLIAMS

Department of Physics, University College of Wales, Penglais, Aberystwyth SY23 3BZ, UK

Abstract

Systematic studies of the upper atmosphere by the so-called incoherent-scatter technique have now been conducted at a limited number of sites for more than a decade. This article reviews the history of the development of the technique, the basic theory involved and the atmospheric parameters which have been successfully measured, together with a summary of existing facilities and current developments.

This review was received in July 1977.

0034–4885/78/0006-0909 $05.00

Contents

1. Introduction

Systematic radio studies of the upper atmosphere from the ground started over fifty years ago with the pioneer experiments of Appleton and Barnett (1925). The principle of their experiment was closely analogous to that of Lloyd's mirror interference experiment in optics. The direct ground signal to the receiver from a continuous-wave transmitter interfered with an indirect wave reflected from the upper atmosphere. Varying the frequency of the transmitter by a small, known amount produced interference waves at the receiver and a count of these enabled the height of reflection to be determined.

In 1926 Breit and Tuve successfully used pulsed radio signals to observe reflections from the upper atmosphere. A radio transmitter was modulated with pulse signals and at a nearby receiver separate ground and echo signals were recorded. Measurement of the time delay for the echo signal enabled the height of the reflecting layer to be estimated.

These early experiments provided clear evidence that in the upper atmosphere there is a region (subsequently called the ionosphere) where the gases are lightly ionised, so providing a reflecting layer at the appropriate frequency. The refractive index n of a medium of electron density N for a radio frequency f is approximately given by

$$n=(1-e^2N/4\pi^2\epsilon_0 m_e f^2)^{1/2}$$

where e and m_e are the electron charge and the rest mass respectively and ϵ_0 is the permittivity of free space. Substantial reflection of the signal may be expected as n approaches zero and the electron density required to reflect a signal of frequency f is then $N=4\pi^2\epsilon_0 m_e f^2/e^2$.

After numerical values of the constants are inserted, it is seen that an HF signal transmitted vertically from the ground travels upwards until it reaches a level where $N=1{\cdot}24\times10^{-2}f^2$ m^{-3} and it is then reflected. The expression is sometimes written as $f=9\,N^{1/2}$ Hz and f is referred to as the plasma frequency (f_p) appropriate to the electron density N. If the maximum or peak density of free electrons in the ionosphere corresponds to a plasma frequency less than the signal frequency, the signal passes through the ionosphere without reflection, and so the plasma frequency at the peak of an ionised region is also referred to as the critical penetration frequency.

Further studies of the ionosphere showed that it can be conveniently divided into a number of layers or regions: the D region (below 90 km); the E region (90–160 km); and the F region (above 160 km) which, during daytime in local summer, is divided in turn into two layers, F1 and F2. Actual observed magnitudes of the electron density in each region vary considerably with the time of day, season and sunspot cycle but typical values would be about 10^9 m^{-3} in the D region, rising to a maximum of about 10^{12} m^{-3} in the F2 region.

For the first few years of radio investigations of the ionosphere both the continuous-wave (CW) and the pulse technique were used, but in time the simplicity and practical advantages of the pulse method were recognised and from about 1930 onwards the pulse technique was adopted generally for routine soundings. At first pulse recordings were made on selected fixed radio frequencies but within a few years experiments

were carried out in which the carrier frequency was continuously varied over a wide frequency band, the receiver being maintained in tune with the transmitter. Initially the synchronisation between transmitter and receiver was carried out manually, later by mechanical linkage, and finally by electronic techniques. The complete equipment (transmitter, receiver and recorder) is known as an 'ionosonde' and the photographic record of time delay as a function of probing frequency is termed an 'ionogram'. Typical ionograms for summer and winter day conditions at a temperate latitude are shown in figure 1 (plate) where the overall time delay of the echo signal (t_d) gives a measure of the 'equivalent height' (h') of the reflecting layer, using the relationship $h' = \frac{1}{2}t_d c$, where c is the velocity of an electromagnetic wave *in vacuo*. Since the actual velocity of travel of the signal in the reflecting layer is less than c this equivalent height is always larger than the true height of reflection but various methods have been developed for the accurate estimation of true height from the observed equivalent height.

In the period from about 1930 to 1960 these ionograms were the principal source of information about the physical properties of the ionosphere and although in the past twenty years rockets and satellites have provided a great wealth of additional data, radio-sounding stations distributed around the world continue to provide certain valuable basic information. In particular, measurements of the different critical penetration frequencies (indicated in figure 1 as f_0E, f_0F1 and f_0F2) enable the maximum electron densities in the various ionospheric layers to be deduced easily and accurately.

Various techniques have also been developed for using an ionogram to calculate the complete electron density/height or $N(h)$ profile from the lowest part of the ionosphere (about 60 km) to the peak of the F2 layer (at 220–350 km). The $N(h)$ profile obtained from the ionogram shown in figure 1(*b*) is given in figure 2.

The conventional ionosonde has the advantage that echoes can be obtained with pulse transmitters of quite small power and as a result it has been possible to establish a network of more than a hundred ionosondes over the world which provide, at comparatively low cost, very good data on spatial variations of the ionosphere. However, the ionosonde has several limitations.

(*a*) The highest level which can be 'sounded' from the ground is that of the peak electron density in the F2 layer. Many interesting and important ionospheric phenomena occur below the F2 peak but the ionosphere extends upwards well beyond this level, and in fact about two-thirds of the total ionisation occurs in the so-called 'top-side ionosphere'. Ionosondes are also unable to yield unambiguous data on the $N(h)$ profile in the 'valley' which sometimes occurs between the E and F regions.

(*b*) Sometimes ionograms cannot be used to provide $N(h)$ profiles because of the signals scattered by perturbations and irregularities in electron density. Especially serious are the effects of 'sporadic-E' and 'spread-F' (see figure 3 (plate)). The 'sporadic-E layer' is normally found between 100 and 120 km. In its weaker forms, sporadic-E consists of clouds of ionisation, and in its most intense form it appears as a thin sheet of ionisation some tens or hundreds of metres in thickness and tens, or even hundreds, of kilometres in horizontal extent. Irregularities in electron density also cause the 'spread-F' conditions which cause the echo signals from the F2 layer to spread out in both range and frequency.

(*c*) The ionogram provides a measure of one parameter, the variation of electron density with height, but a proper understanding of the ionosphere calls for a know-

ledge of the full range of parameters, including ion composition, ion temperature, electron temperature and plasma drift velocity.

In recent years, ionosonde measurements from the ground have been supplemented in several ways to overcome these limitations. For example, routine radio soundings of the 'top-side' ionosphere have followed the introduction of artificial Earth satellites. In the past 15 years or so a number of top-side radio-sounding satellites have been launched, of which the best known and most successful has been the Canadian satellite Alouette I. This satellite carried a complete miniature version of the ground-based ionosonde and was launched in 1962 into a roughly circular orbit 1000 km above the Earth. Over a period of several years of faultless operation it produced more than a million high-quality top-side ionograms. Figure 4 shows an $N(h)$ profile covering the height range 0–1000 km obtained by combining data from bottom- and top-side ionograms.

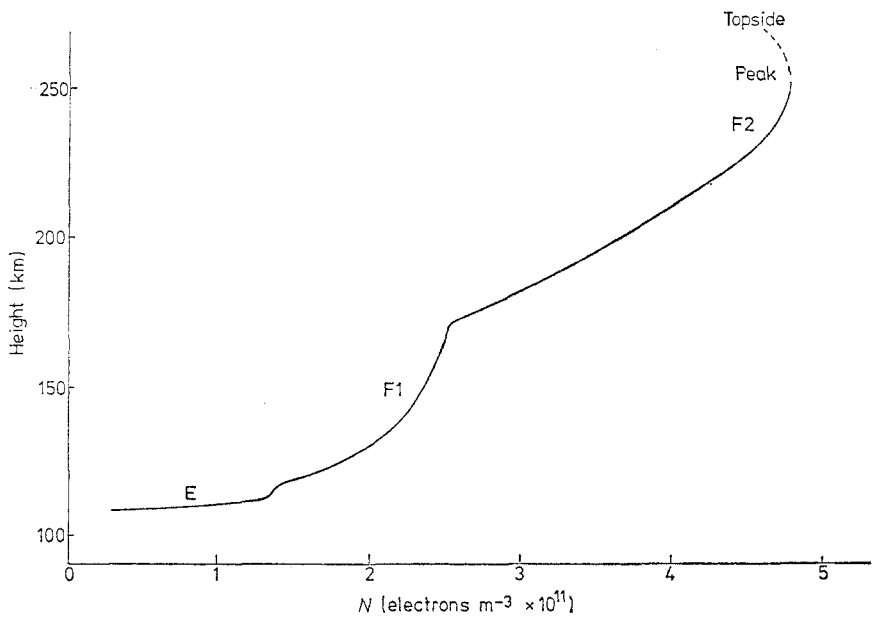

Figure 2. Electron density/height profile corresponding to the ionogram shown in figure 1(*b*).

Such satellites give good global coverage for a considerable range of altitudes, but observations at any one location are only repeated after a long interval. Moreover, an orbiting satellite is unable to distinguish spatial and temporal changes. This is an especial limitation in the auroral zone where rapid spatial and temporal changes are frequently encountered.

Rockets can also cover a wide range of altitudes, from the base of the D region, through the E and F regions into the top-side. Rockets are well suited to measuring a wide range of parameters including electron and ion temperatures, ion composition and the energy spectrum of precipitated particles. However, rockets are expensive and each rocket only provides a sounding over a time interval of a few minutes at one location. Frequent measurements with rockets over a long period thus present formidable difficulties. Nevertheless, in the last thirty years many thousands of rocket experiments have been carried out and collectively have made a very substantial contribution to present knowledge of the upper atmosphere.

However, the most important development in recent years in ground-based sounding has been the introduction of 'incoherent-scatter' radar. In this connection it is relevant to note that in 1968 URSI (the International Union of Radio Science) established an expert Working Group to survey critically the whole field of electromagnetic probing of the atmosphere. The report of the Group was published in 1970 and several of the individual contributors stressed the importance of the incoherent-scatter technique. Thus Booker and Smith (1970) concluded:

'The incoherent-scatter radar appears to be providing the most accurate and convenient means for measuring ion temperature, electron temperature, electron

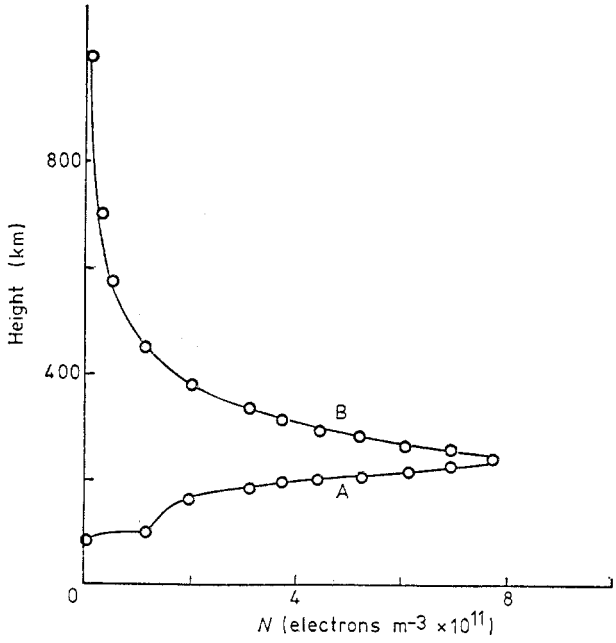

Figure 4. Combination of electron density profiles derived from A, a bottom-side sounder (Port Stanley ionosonde), and B, a top-side sounder at 1000 km (Alouette I) (after W Becker, private communication).

density and plasma drift velocity between one hundred and several hundred kilometres. Moreover, from these quantities may be derived important information about the electric field, the neutral wind, the neutral temperature, the vertical fluxes of particles and of heat, the photoelectron energy and the composition of the atmosphere.

'If second-generation incoherent-scatter radars can be adequately deployed in the next decade, they should revolutionise aeronomy in the altitude range from about 100 to 1000 km and make major contributions to the dynamics of the magnetosphere.'

The remainder of this review describes the development of incoherent-scatter radar and its application to studies of the high atmosphere.

Additional material on incoherent scatter will be found in the following review papers: Evans (1969, 1974), Farley (1970) and Beynon (1974).

2. History of incoherent-scatter radar

In 1906 J J Thomson showed that free electrons are capable of scattering electromagnetic radiation in a particular direction with a scattering cross section of $\sigma = 4\pi(r_e \sin \gamma)^2$ where r_e is the electron 'radius' ($= \mu_0 e^2/m_e$) and γ is the angle between the direction of the incident electric field and the direction to the observer. For a direct back-scatter, γ would be 90° so that a free electron would have a scattering cross section of $\sigma_e = 0{\cdot}998 \times 10^{-28}$ m^2.

In the earliest days of radio sounding of the ionosphere Fabry (1928) suggested that the scattering of electromagnetic waves by free electrons in the ionosphere might be significant at radio frequencies. He also pointed out that if the electrons were illuminated by a monochromatic beam the scattered signal would show a Doppler broadening corresponding to the thermal velocity of the electrons. Beyond emphasising that the scattering cross section of electrons was extremely small, Fabry made no attempt to estimate the strength of the scattered radio signal for a transmitter of given power: had he done so, it would have been clear that with the transmitter power and receiver sensitivities available at that time there would have been no chance whatever of detecting such weak signals. This can be quickly appreciated from an estimate of the total effective scattering cross section. Near the peak of the ionosphere, at about 300 km altitude, the electron density is of the order of 10^{12} m^{-3} so that the effective scattering cross section from a cubic metre is only 10^{-16} m^2, and even a cube of side 10 km has a total effective cross section of only 10^{-4} m^2. In other words, as pointed out by Ratcliffe (1972), the problem is equivalent to that involved in detecting a small coin at a range of several hundred kilometres.

In the 1950s, however, following the wartime development of very high-power radar systems, this was clearly attainable and in 1958 Gordon suggested that a large enough antenna would make it possible to detect the Thomson scattering of radar signals from the ionosphere, and to measure both electron density and electron temperature as a function of height.

The simple theory of scattering may be outlined here. Consider a volume of plasma $A\,\mathrm{d}h$, of horizontal cross section A and thickness $\mathrm{d}h$ at a vertical range h, so that the number of scattering electrons in this volume is $N(h)\,A\,\mathrm{d}h$. If the plasma is illuminated by a transmitted signal of wavevector $\boldsymbol{k}$ and the scattered radiation is received at the same site as the transmitter, then the total phase change during travel will be $(2\,\boldsymbol{k}.\boldsymbol{h})$. We can therefore represent the signal scattered from the volume of plasma as:

$$s(\boldsymbol{k}.\boldsymbol{h}) = \text{constant} \times N(h)A\,\mathrm{d}h \exp(2\mathrm{i}\,\boldsymbol{k}.\boldsymbol{h}).$$

Hence the total signal at the receiver scattered from the range h_1 to h_2 is:

$$S(\boldsymbol{k}) = \text{constant} \times \int_{h_1}^{h_2} AN(h) \exp(2\mathrm{i}\boldsymbol{k}.\boldsymbol{h})\,\mathrm{d}h$$

which corresponds to the Fourier transform of $N(h)$ over the range h_1 to h_2.

If the plasma consists of free thermal electrons, distributed at random with a constant average density corresponding to a mean spacing of δ, then the Fourier transform of $N(h)$ will be independent of k provided $|k| \ll 2\pi/\delta$. In other words, when the electrons are totally independent of each other the incident wave is scattered equally for all wavelengths λ provided $\lambda \gg \delta$. In the ionosphere, for the height range 100–2000 km, δ is always less than 10^{-3} m and this condition is readily met. Simple theory thus suggests that because of their random motions the electrons scatter

signals with random phases so that at the receiver the signal powers add rather than the signal voltages, and the scattering is truly incoherent. It follows that the total power scattered by a given volume is proportional to $\sigma_e N(h)$ so that if the scattered power is measured, $N(h)$ can be determined.

If, however, there are comparatively large-scale variations in $N(h)$, corresponding to a 'corrugation' wavelength Λ in the direction of observation, then the scattered signal will reach a sharp maximum for radiation of wavelength $\lambda = 2\Lambda$, which corresponds to constructive interference or coherent scattering. In order to avoid coherent or partially coherent scattered radiation we must choose an observing wavelength much shorter than the scale of the smallest irregularities which exist in the electron density distribution in the ionosphere. Structures with a scale size of tens of metres are known to occur under certain conditions—in the auroral zone, for example, or associated with 'spread-F' at the peak of the ionosphere—and in order to avoid contamination of the very weak incoherent echoes by traces of the much stronger coherent echoes it is usual to choose an observing wavelength $\lambda \lesssim 1$ m.

In his original proposal, Gordon did not consider the possibility of coherent or quasi-coherent echo signals from ionospheric irregularities, and he anticipated that incoherent-scatter signals from individual electrons might be observed at a wavelength of 1·5 m. He also expected that the spectrum of the scattered signal would be spread over a bandwidth of several hundred kHz. Simple theory predicts that due to their random thermal motions, the electrons would scatter the radiation with a wide range of Doppler shifts, so that the spectrum of the scattered signal would be Gaussian in shape with a half-power bandwidth of

$$\Delta f = 4(kT_e/m_e\lambda^2)^{1/2} \text{ Hz} = 15{\cdot}6\ T_e^{1/2}/\lambda \text{ kHz}$$

where k is Boltzmann's constant and T_e is the electron temperature, i.e. for $\lambda = 1{\cdot}5$ m and $T_e = 1600$ K, the total half-power bandwidth would be over 400 kHz.

In 1958, Bowles reported the first actual observations of echoes using a newly constructed high-power transmitter at Long Branch, Illinois. He found that the total scattered power was of the magnitude predicted by Gordon, but the bandwidth was very much smaller and, hence, the scattered power per unit bandwidth very much greater. Bowles correctly suggested that the observed Doppler spread corresponded to the thermal velocities of the much heavier positive ions present in the high atmosphere, rather than of the electrons themselves. In other words, the power scattered corresponded to the cross section of the *electrons* but the spectrum corresponded to the thermal velocities of the *ions*. It was clear that a new theory was required to explain the observed signals. Several authors, including Fejer (1960), Dougherty and Farley (1960), Salpeter (1960a, b) and Hagfors (1961), tackled the problem independently with results which were in substantial agreement. Moreover the new theories suggested that several additional parameters could be determined from a careful analysis of the observed spectrum.

3. Theory of 'incoherent' scatter

The new theories recognised that in the ionosphere it is inappropriate to consider 'free' electrons because of the electrostatic forces between electrons and neighbouring positively charged ions. Because of these forces, ions tend to be attracted towards

each electron while at the same time their thermal velocities and their mutual repulsion tend to disperse them. As a result, the ions form a shielding layer around each electron, the scale of which is determined by the balance between random thermal energy and electrostatic potential energy and is quantitatively represented by the Debye length:

$$D=(\epsilon_0 kT_e/Ne^2)^{1/2}=69(T_e/N)^{1/2}\text{ m}.$$

In the ionosphere T_e and N clearly depend on altitude, time of day, season and degree of solar activity. Consideration of these various factors show how the value of D varies. Minimum values of about 0·3 cm occur at the peak of the F region ($\sim$250 km) with values of 6 cm or more in the lower E region ($\sim$90 km) or at very great heights ($\sim$2000 km).

If the radar wavelength is very much smaller than D then we can indeed consider scattering by 'free' electrons and the observed spectrum will agree with Gordon's prediction, having a half-power bandwidth of several hundred kHz. However, when the exploring wavelength is very much greater than D, as is usually the case, we can no longer consider scattering from free and independent electrons because, as stated above, the movements of the electrons are strongly controlled by the surrounding ions. As a result of electrostatic coupling, the random thermal motions of the electrons generate waves in the plasma known as 'ion-acoustic' waves and 'electron-acoustic' or 'plasma' waves. These waves resemble acoustic waves in a neutral gas where pressure gradients give rise to longitudinal waves. In the case of a plasma similar waves occur, but when the density of ions (or electrons) increases locally a net electric charge is produced, and electrostatic forces must be added to the forces due to pressure gradients. It is the fluctuation of electron density caused by such waves that actually give rise to the observed scattered signals.

These waves occur over a wide and continuous spectrum of wavelengths propagating in all directions and they include waves with a wavelength $\Lambda=\frac{1}{2}\lambda$, travelling upwards or downwards along the direction of the radar beam at a velocity V; such waves cause a very strong 'quasi-coherent' scattered signal which can be received at the ground. If the signal is scattered by an upward travelling wave it will experience a Doppler frequency shift:

$$\Delta f=-2V/\lambda=-V/\Lambda=-F(\Lambda)$$

where $F(\Lambda)$ is the frequency of the wave. Similarly, the signal scattered by a downward travelling wave will experience a Doppler shift $=+F(\Lambda)$. Given the existence of both ion-acoustic and electron-acoustic waves travelling upward and downward, it follows that the spectrum of the scattered signals will consist of four components centred at the following frequencies: $f\pm F^+(\Lambda)$ and $f\pm F^-(\Lambda)$, where $F^+(\Lambda)$ and $F^-(\Lambda)$ are the frequencies of the ion-acoustic and electron-acoustic waves respectively. Theory shows that

$$F^+(\Lambda)=[(kT_i/m_i)(1+T_e/T_i)]^{1/2}/\Lambda$$

and

$$F^-(\Lambda)=f_p(1+12\pi^2D^2/\Lambda^2)^{1/2}$$

where T_i is the ion temperature, m_i is the ion mass and f_p is the plasma frequency of the medium.

The shape of each spectral line depends on the degree of damping that each wave experiences, the main mechanism of attenuation being Landau damping. When

charged particles in a plasma are moving in the same direction as a wave, but at speeds very slightly less than the wave velocity, energy will be transferred from the wave to the particles; the particles will be accelerated and the wave attenuated. If, on the other hand, the particles are moving at a speed very slightly greater than the wave, they will feed energy into the wave and the wave will be enhanced.

It happens that the velocity of the ion-acoustic wave (V^+) is well within the Maxwell distribution of thermal ions at a temperature T_i, and so there are always more ions travelling at a slightly slower speed than at a slightly higher (see figure 5). The ion-acoustic wave is therefore attenuated and as a result the two spectral lines are broadened and in fact merge to give a characteristic 'double-hump' ion spectrum (see figure 6). If we now keep T_i constant but increase T_e, then the velocity of the

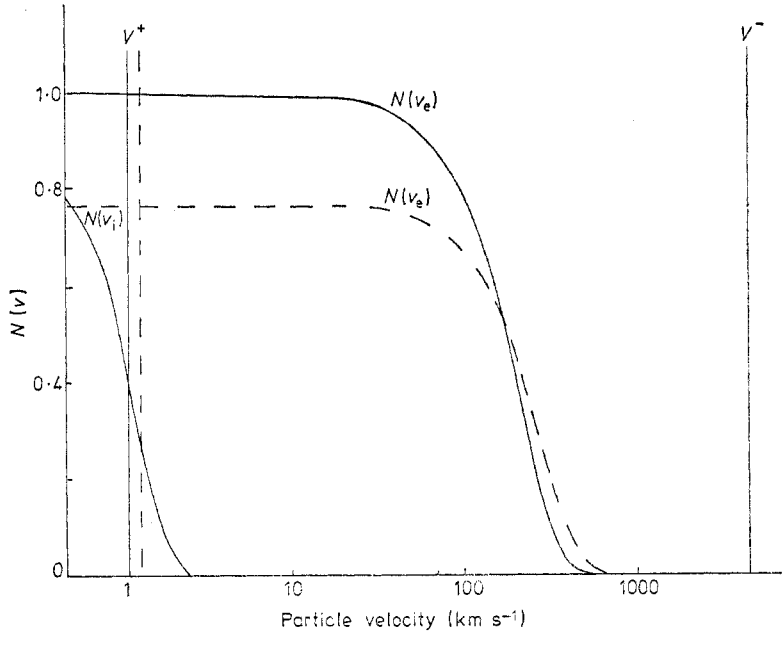

Figure 5. Velocity distribution of thermal electrons $N(v_e)$ and thermal ions $N(v_i)$ and the phase velocity of electron-acoustic (V^-) and ion-acoustic (V^+) waves. $N(v_e)$ and $N(v_i)$ are normalised so that $N(0)=1$ in each case. $N=10^{12}$ m^{-3}, $\lambda=1$ m, $M_i=16$, $T_i=1000$ K, $T_e=1500$ K (———), $T_e=2500$ K (— — —).

ion-acoustic wave increases. As a result, the spectrum of ion velocity in the neighbourhood of the ion-acoustic wave velocity becomes less steep and so the degree of attenuation is reduced and the two peaks in the ion spectrum become sharper, i.e. as the ratio T_e/T_i increases the peaks in the ion spectrum become sharper (figure 7).

The electron-acoustic or plasma waves travel at a far greater velocity, greater in fact than the thermal velocities of the vast majority of electrons, so that there is very little attenuation. On the contrary, if there is a significant influx of suprathermal electrons, such as photoelectrons, and these are travelling at a slightly greater speed than the electron-acoustic waves then the waves will be enhanced and the corresponding plasma lines in the spectrum will remain very sharp.

The typical 'incoherent-scatter' spectrum therefore consists of a double-humped ion spectrum, distributed on either side of the transmitted frequency (f), and two

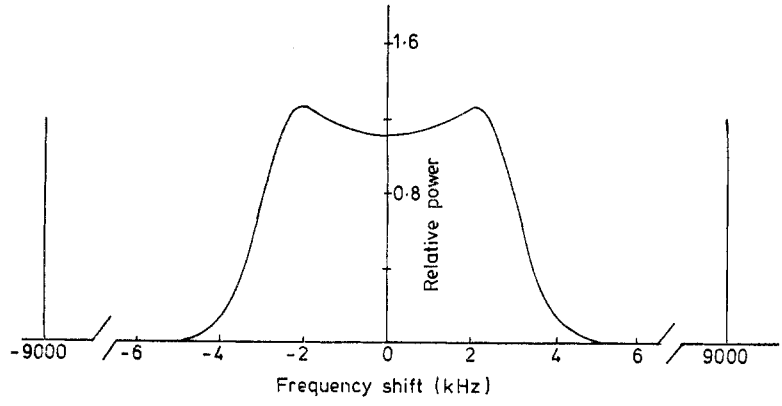

Figure 6. Ion spectrum and plasma lines. $N=10^{12}$ m^{-3}, $T_e=1000$ K, $T_i=1000$ K, $\lambda=1$ m, $M_i=16$.

sharp plasma lines at frequencies $f \pm F^{-}(\Lambda)$. For the radar frequencies used in incoherent-scatter experiments $\lambda \gg D$ so that $F^{-}(\Lambda) \approx f_p = 9N^{1/2}$ Hz. Under normal circumstances, the bulk of the scattered power is in the ion spectrum. Theory shows that the total scattered power corresponds to a scattering cross section per unit volume of σN, where:

$$\sigma = \sigma_e\{1-(1+\alpha^2)^{-1}+[(1+\alpha^2)(1+\alpha^2+T_e/T_i)]^{-1}\}$$

and $\alpha = 4\pi D/\lambda$ (Buneman 1962). For $\lambda \gg D$ this reduces to:

$$\sigma = \sigma_e(1+T_e/T_i)^{-1}$$

which is of the same order as that predicted by simple Thomson theory. If, however, there is an influx of suprathermal electrons, or if the plasma is excited by a strong incident radio wave at the plasma frequency (see §8.2), then the plasma lines can become prominent.

The theory of scattering thus turns out to be considerably more complicated than originally suspected, but it is now well established. It is clearly not a simple theory of incoherent scattering by free electrons; rather, it describes quasi-coherent scattering by thermally induced electron–ion acoustic waves. Nevertheless, no new name has yet been agreed for the process and it is still universally referred to

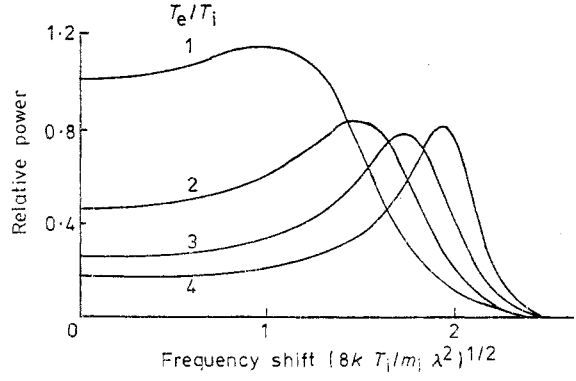

Figure 7. Dependence of ion spectrum on T_e/T_i.

as 'incoherent scatter'. For brevity, in the remainder of this review we shall use the abbreviation IS.

4. Parameters measured by IS

If the complete spectrum of the scattered signal is measured with adequate signal-to-noise ratio it is possible to determine, with greater or lesser precision, up to eight parameters of the scattering volume, viz electron density, electron temperature, ion temperature, ion mass, plasma drift velocity, ion–neutral collision frequency, part of the spectrum of suprathermal electrons, and electric current. Once these have been determined at least six other parameters can be calculated, viz static electric field strength, Hall and Pedersen conductivities, the wind speed and temperature of the neutral atmosphere, and the downward flux of heat. Several of the parameters are interdependent and sometimes the determination of one depends on prior knowledge of another or in other cases the parameter can only be determined provided assumptions can be made. As with a jigsaw the more pieces in place the easier it is to complete the picture.

4.1. Electron density, $N(h)$

Electron density can be determined as a function of height in three independent ways.

(i) The total power scattered from a height h and received at the aerial ($P(h)$) is equal to

$$K\sigma N(h)/h^2 = K\sigma_e \sin^2 \gamma N(h)/(1+T_e/T_i)h^2$$

where K is a constant proportional to the power transmitted and to the effective collecting area of the receiving antenna (see §6.1). If, therefore, the power scattered from a given height is measured, and if T_e/T_i is known (see §4.2 below) then we can determine $KN(h)$. The equipment constant K can be obtained by measuring $KN(h)$ for the peak of the F2 layer and independently measuring $N(h)$ from f_0F2, the critical frequency of the F2 layer, using an ionosonde. Figure 8 shows an $N(h)$ profile determined in this way at Jicamarca, Peru, extending out to more than 1 Earth radius.

(ii) A signal travelling through an ionised medium in a magnetic field experiences a rotation in its plane of polarisation, the so-called 'Faraday rotation' (Ω), where

$$\Omega = (e^3/8\pi^2 m_e{}^2 f^2 c\epsilon_0)\int N(h)B(h)\cos\beta(h)\,dh$$
$$\simeq 2{\cdot}37\times 10^4 f^{-2}\langle B\cos\beta\rangle\int N(h)\,dh \text{ radians}$$

where B is the magnetic flux density, β is the angle between the path of the signal and the field lines, and the brackets $\langle\ \rangle$ indicate an average value. Therefore

$$d\Omega/dh = 2{\cdot}37\times 10^4 f^{-2}\langle B\cos\beta\rangle N(h) \text{ radians}$$

so that if we know the average value of $B\cos\beta$, we can determine $N(h)$ from $d\Omega/dh$. In IS experiments there is, of course, two-way transmission through the medium and the total rotation is twice that given above.

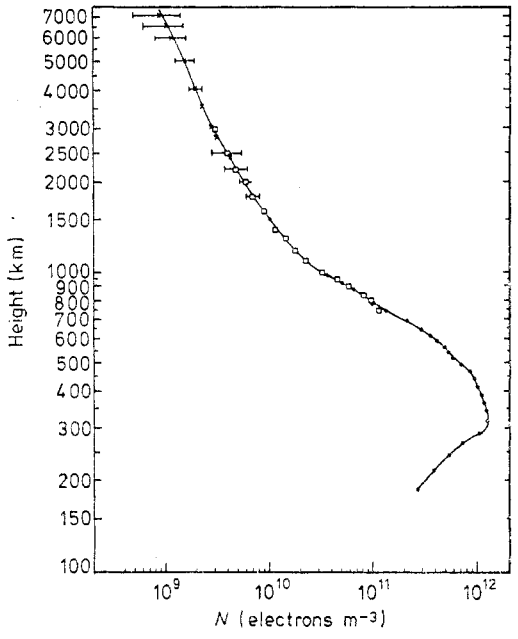

Figure 8. $N(h)$ profiles from 200 to 7000 km at Jicamarca, Peru on 25 April 1962 (after Bowles 1963). ×, 1355 EST; □, 1405 EST; ●, 1415 EST.

In principle this method is very simple, but the simplicity is partly offset by the need to maintain equal gain and perfect orthogonality in the phase-sensitive detectors used to measure the polarisation of the scattered signal. Any coupling between the right-handed and left-handed modes of polarisation must also be less than −25 dB. These errors can be eliminated by introducing an extra phase of 90° into each detector in turn (i.e. by interchanging the detectors) and by introducing an extra phase of 180° into one of the modes at the transmitter (Farley *et al* 1967). This method gives an absolute measurement of N but the errors become larger when $d\Omega/dh$ becomes small, as at high altitudes.

(iii) For a wavelength much greater than the Debye length, the electron component of the spectrum consists of two plasma lines displaced from the transmitted frequency by approximately $\pm f_p = \pm 9N^{1/2}$. Normally at night these lines are too weak to be detected, but in daytime they can be enhanced up to 50-fold by the effect of fast photoelectrons or secondary auroral electrons. They can also be stimulated artificially by transmitting a powerful radio signal at the plasma frequency (f_p) (Carlson *et al* 1972). At the Arecibo Ionospheric Observatory the $N(h)$ profile has been determined by offsetting the frequency of the receiver at a series of preselected values of f_p and locating the heights of the corresponding plasma lines (figure 9(*a*)). Observations of the plasma lines have also been made at the Nancay Observatory in France using a receiver with a series of frequency filters (figure 9(*b*)).

4.2. The ratio of electron and ion temperature, T_e/T_i

Among the thermal ions of a plasma, the distribution of velocity in a given direction, $N(v_i)$, varies as $T_i^{-1/2} \exp(-m_i v_i^2/2kT_i)$. The velocity of the ion-acoustic

wave in the same direction (V) equals $[(kT_i/m_i)(1+T_e/T_i)]^{1/2}$. Now as mentioned above Landau damping depends on the gradient of the ion velocity distribution at the velocity of the ion-acoustic wave and from this it follows that the 'sharpness' of the ion lines depends on T_e/T_i. If, therefore, the frequency scale of the scattered spectrum is normalised by dividing the frequency shift by $(8kT_i/m_i\lambda^2)^{1/2}$, i.e. the Doppler shift of ions moving with the mean thermal velocity corresponding to T_i, the IS spectrum can be reduced to a standard form where the only variable para-

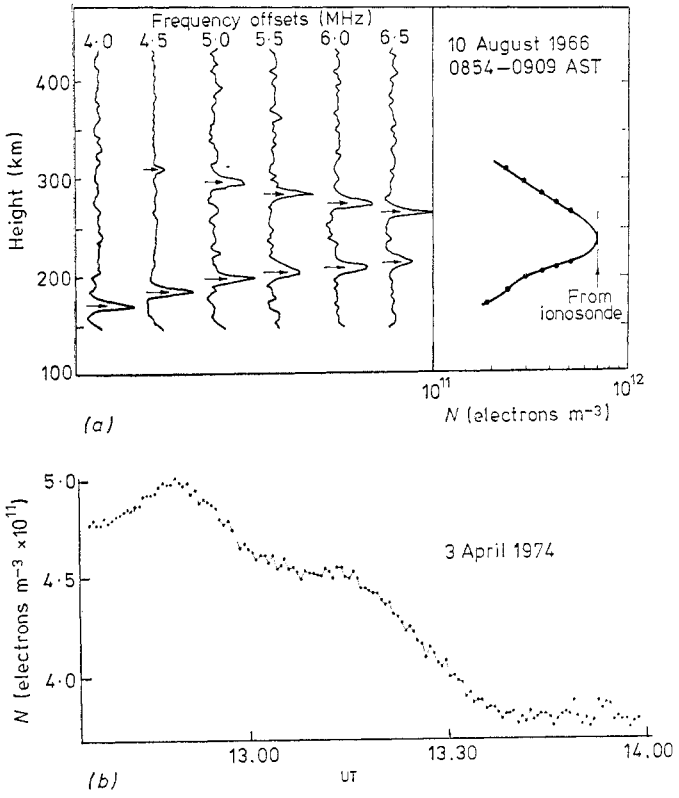

Figure 9. (*a*) Determination of electron density from observations of plasma lines: variation with height at Arecibo (from Wand 1970). (*b*) Determination of electron density from observations of plasma lines: variation with time at a fixed height (300 km) at St Santin (after Vidal-Madjar *et al* 1975).

meters are $N(h)$ and T_e/T_i. Figure 7 shows clearly that the ratio of the peak power to the power in the trough of the ion spectrum is very sensitive to T_e/T_i, and so a measurement of the full ion spectrum gives the ratio T_e/T_i.

Alternatively, the total scattered power from a given height, $P(h)$, can be measured and $N(h)$ determined by one of the alternative methods, viz by Faraday rotation, or by measuring the frequency of the plasma lines. The ratio T_e/T_i can then be determined from the expression $P(h)=K\sigma_e \sin^2\gamma N(h)/(1+T_e/T_i)h^2$. Figure 10 shows excellent agreement between profiles of T_e/T_i measured by the ion spectrum and the plasma line methods.

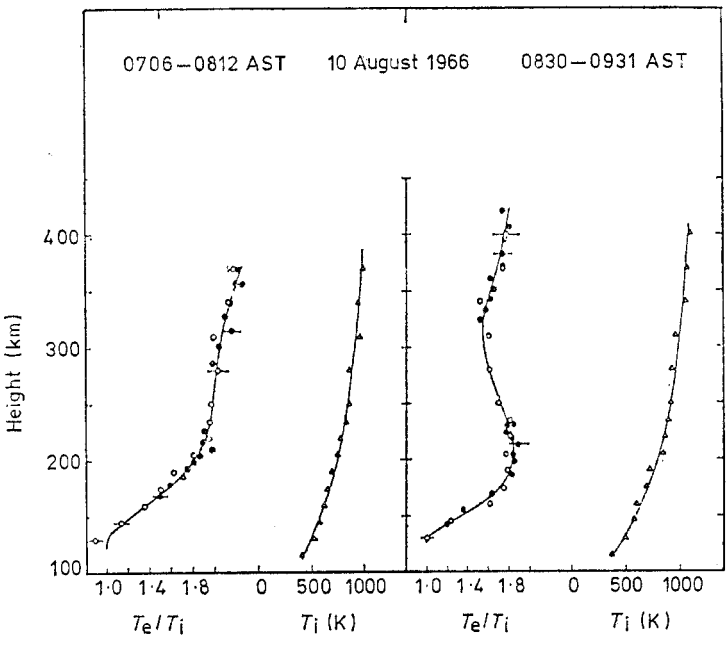

Figure 10. T_e/T_i measured from ion spectrum (○) and plasma lines (●). T_i from ion component (△).

4.3. The ratio of ion temperature and ion mass, T_i/m_i

The separation of the two ion lines in the IS spectrum:

$$2F^{+}(\Lambda)=4[(kT_i/m_i)(1+T_e/T_i)]^{1/2}/\lambda.$$

Hence, if the ratio T_e/T_i is known, T_i/m_i can be determined from the separation of the two maxima of the ion spectrum or from the half-power bandwidth. If now m_i can be assumed, the absolute value of T_i can be established and hence T_e.

In the lower E region of the ionosphere, from 90 to 140 km, O_2^+ and NO^+ ions are dominant and as their masses are similar, even a rough estimate of the relative proportions of O_2^+ and NO^+ is sufficient to determine m_i to an accuracy of better than 1%. Reliable assumptions about the value of m_i can also be made for altitudes near the F2 peak, where undoubtedly the dominant ion is O^+, and again at very great altitudes where the ion population is entirely composed of protons. Where such assumptions can be made, it is possible to determine T_e and T_i and figure 11 shows routine temperature measurements made at Millstone Hill.

4.4. The ion mass, m_i

As we have seen, for certain height ranges the value of m_i can be reliably estimated and hence T_i and T_e determined. In the transition height ranges the problem is more difficult but fortunately the spectrum of the scattered signal from a plasma containing two different ion species is not simply the spectrum corresponding to the mean ion mass. When two ion species are present, and these have substantially different ion mass, a new family of theoretical spectra can be derived (figure 12). It is seen that the slope of the spectrum at the half-power points is a useful indicator

of the percentage composition. Alternatively, T_i can be measured in those height ranges where m_i is known with certainty, and by interpolating a profile of T_i in the transition ranges the variation of $\langle m_i \rangle$ with height can be estimated, and hence the composition of the ions at each height (Petit 1968, Evans 1969). Such methods have been used to observe the transition from molecular ions (O_2^+ and NO^+) to atomic ions (O^+) in rising from the E to the F region, or the transition from O^+ to the lighter ions of H^+ (and He^+) in the top-side ionosphere. Figure 13(*a*) illustrates the transition from molecular to atomic ions observed at St Santin. Similar results for this transition level and its seasonal variation have been reported from Millstone Hill (Cox and Evans 1970). In theory it should also be possible to determine the percentage of each of three ions present (from the shape of the spectrum) but this

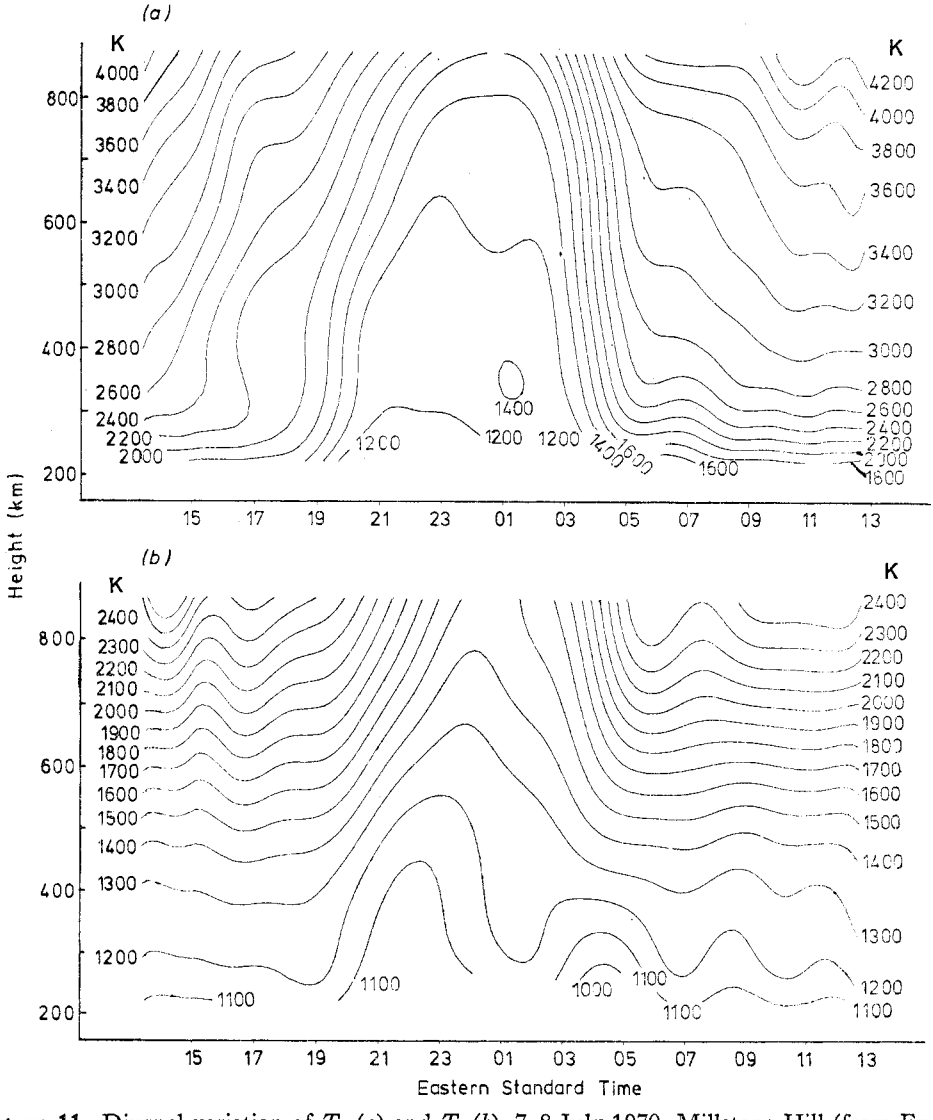

Figure 11. Diurnal variation of T_e (*a*) and T_i (*b*), 7–8 July 1970, Millstone Hill (from Evans and Holt 1976).

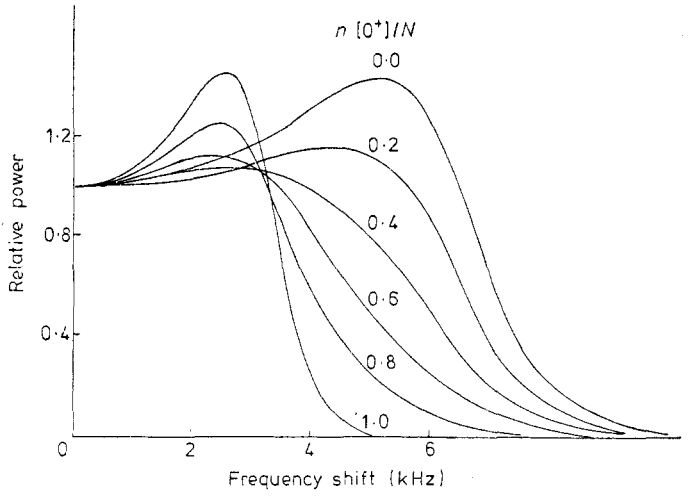

Figure 12. Ion spectrum for different mixtures of O^+ and He^+ (from Moorcroft 1964). $T_e = 1500$ K, $T_i = 1000$ K, $\lambda = 1$ m.

calls for an extremely good signal-to-noise ratio, and only at Arecibo have reliable three-ion measurements been made (figure 13(*b*)).

4.5. Plasma velocity, V_p

All the preceding theory applied to scattering from a plasma at rest. If there is a bulk movement of the plasma, the spectrum as a whole is Doppler-shifted but otherwise unchanged. By measuring the mean Doppler shift of the scattered spectrum the component of plasma velocity in the 'mirror' direction ($V_{p,\,m}$) can be determined (figure 14). The mean shift ($= -2\,V_{p,\,m} f/c$) is small compared with the width

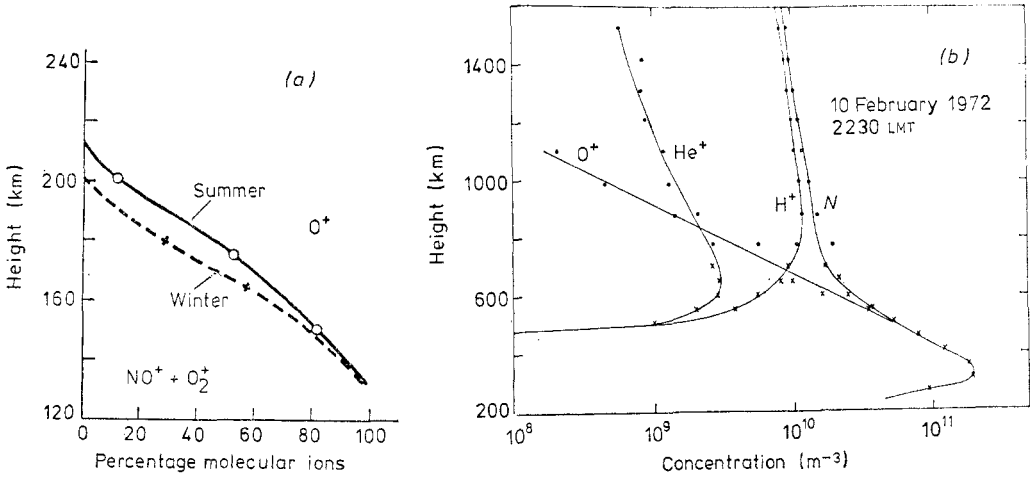

Figure 13. (*a*) Relative concentrations of ions with height: transition from molecular ions [$NO^+ + O_2^+$] to atomic ions [O^+] observed at St Santin (from Waldteufel 1970). (*b*) Relative concentrations of ions with height: O^+, He^+, H^+ at Arecibo. The concentration of electrons (N) is also shown (from Hagen and Hsu 1974).

of the ion spectrum. For example, the ion spectrum of a plasma of O^+ ions where $T_e = 1500$ K and $T_i = 1000$ K has a half-power width of about 9 kHz when observed at 400 MHz. If the plasma is moving in the mirror direction at a velocity of ~ 100 m s^{-1}—a large velocity for mid and low latitudes—the mean Doppler shift will be less than 0·3 kHz. An accurate measurement of the whole spectrum is therefore required to measure $V_{p,\,m}$ though it is the steep sides of the spectrum that are

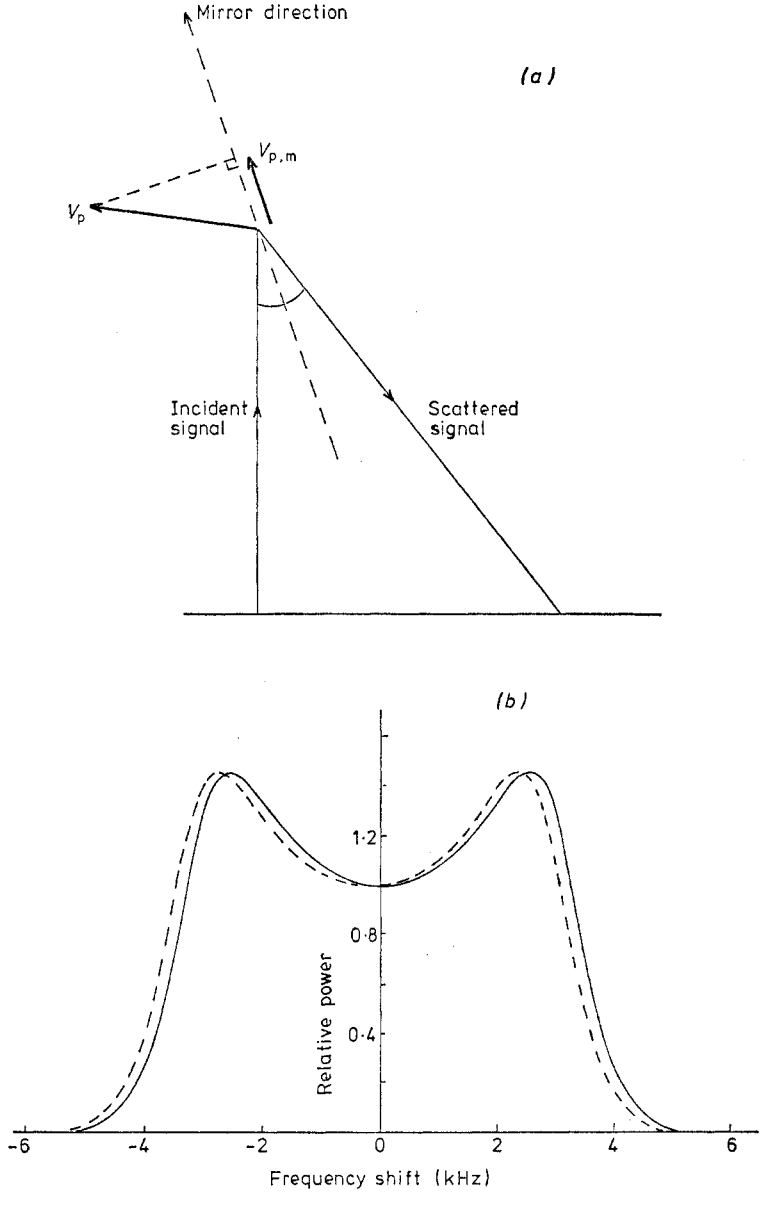

Figure 14. (*a*) The mirror direction for a bistatic system, showing the component of plasma drift velocity ($V_{p,\,m}$) measured by such a system. (*b*) Ion spectrum for zero plasma velocity (———) and for a plasma velocity of 100 m s^{-1} in the mirror direction (— — —). $T_e = 1500$ K, $T_i = 1000$ K, $M_i = 16$ (O^+), $\lambda = 1$ m.

most sensitive to the Doppler shift (figure 14(*b*)). If measurements of this kind are made simultaneously at three separate receiving stations suitably located, the three components of plasma drift velocity can be combined to give the true drift velocity of a single volume of plasma.

The parameters listed above may all be derived as a routine from the spectrum of the scattered signal, and several stations publish measurements of N, T_e, T_i and V_p on a regular basis.

Three other parameters may be determined directly from the spectrum, but only for a limited range of heights or under favourable circumstances.

4.6. Ion–neutral collision frequency, ν_{in}

Above about 140 km the frequency of an ion-acoustic wave propagating in the plasma, $F^+(\Lambda)$, is much greater than the ion–neutral collision frequency, ν_{in}, so that Landau damping by thermal ions is the main mechanism of attenuation.

In moving to lower altitudes, however, T_i tends to decrease and m_i increases so that $F^+(\Lambda)$ falls steadily while ν_{in} increases sharply in proportion to the density of the neutral atmosphere.

When eventually $\nu_{in} \gg F^+(\Lambda)$, the ion-acoustic waves can no longer propagate and the spectrum loses its double-humped appearance, becoming narrower in the process. For an observing wavelength λ, the shape of the spectrum is determined by a parameter $\psi_i = \lambda/4\pi l_i$ where the mean free path of the ions $l_i = (2kT_i/m_i)^{1/2}/\nu_{in}$ (figure 15).

At these heights $T_e = T_i = T_n$ (the neutral temperature) so that the width of the spectrum will be proportional to $T_i^{1/2}$ and the shape will depend on $\nu_{in} T_i^{-1/2}$. Hence measurements of the width and shape enable both T_i and ν_{in} to be determined as a function of height. Profiles of T_i and ν_{in} over the height range 100–120 km are shown in figure 16.

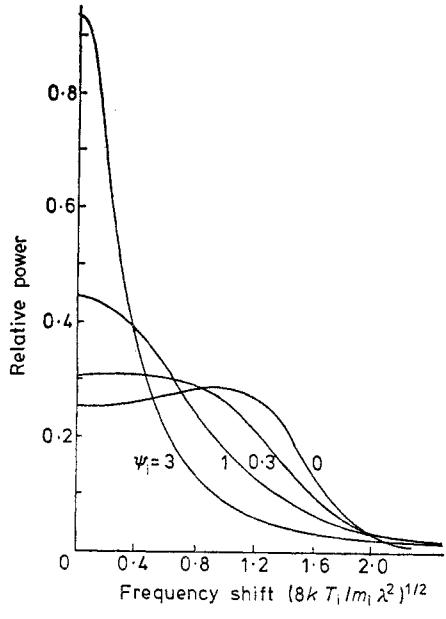

Figure 15. Influence of collisions on ion spectrum (from Dougherty and Farley 1963).

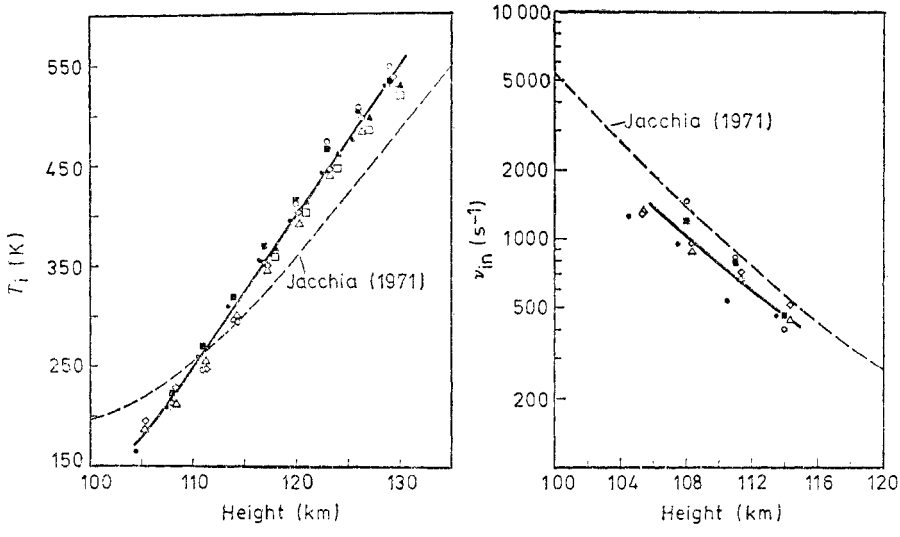

Figure 16. Average daytime ion temperature and ion–neutral collision frequency obtained at Arecibo (from Evans 1974). Also shown are the values obtained from the Jacchia (1971) model. ▲, 27 March 1969; □, 28 March 1969; ●, 22 September 1970; ■, 24 September 1970; ○, 26 September 1970; ◇, 30 September 1970; △, 3 October 1970.

4.7. Spectrum of suprathermal electrons

Suprathermal electrons travelling at velocities slightly greater than the phase velocity of an electron-acoustic wave transfer energy to the wave. Furthermore photoelectrons or secondary auroral electrons in the energy range 1–50 eV can stimulate 'plasma' lines and the strength of these lines is an indication of the slope of the electron velocity distribution at the appropriate velocity ($\approx f_p\lambda/2$).

Above the peak of the F2 layer we can assume that for energies greater than 6 eV the spectrum is practically height-independent (apart from a known magnetic-field factor), while the plasma phase velocity ($f_p\lambda/2$) varies. Measurements at different altitudes where the electron density, and hence f_p, are different can therefore be combined to give part of the spectrum of precipitation suprathermal electrons (Yngvesson and Perkins 1968).

There are two restrictions to the range of heights that can be covered. Landau damping by thermal electrons sets a minimum plasma frequency at which the lines may be detected (figure 5), while ion–electron collisions set a maximum frequency. Theory thus shows that the lines are only observed in the height range where $2/\lambda < f_p < 6/\lambda$ MHz†. If, however, the plasma lines can be observed using two or more different radar frequencies the height range covered can be extended (see §8.1). Figure 17 shows a photoelectron flux spectrum measured at Millstone Hill for an altitude of 540 km together with spectra measured by satellites OV1–18 at 560 km and ISIS 1 at 2770 km. The three sets of data refer to approximately the same solar zenith angle but some allowance should be made for differences in solar activity on the three dates concerned. Furthermore, for comparison with the Millstone Hill IS values the flux measured by the ISIS 1 satellite at 2770 km should be

† Some recent observations suggest that under certain circumstances the restriction $f_p > 2/\lambda$ may not always apply.

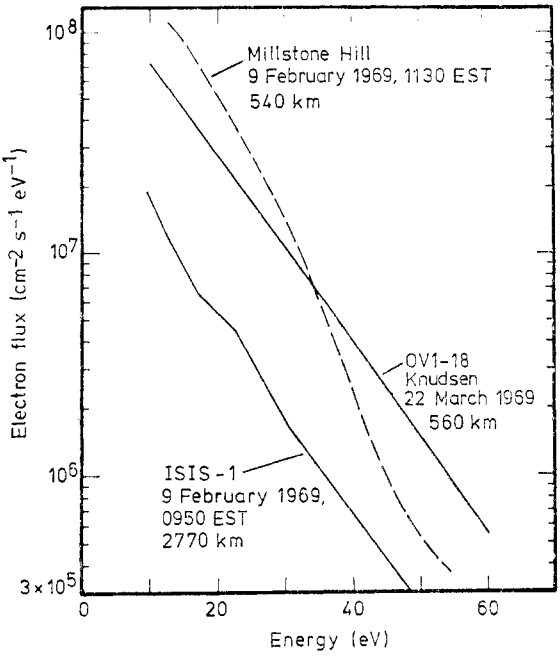

Figure 17. Photoelectron flux spectra measured at Millstone Hill for an altitude of 540 km and on satellites at 560 and 2770 km (from Cicerone 1974).

multiplied by a factor of about three to allow for the height variation in the strength of the magnetic field (Cicerone 1974).

4.8. Electric current density, j

If there is a bulk movement of the plasma as a whole, both the ion lines and the plasma lines will be Doppler-shifted by an equal amount. If, however, there is a current flowing this will be equivalent to a difference in the mean drift velocities of the ions and the electrons which will be reflected in a difference between the mean shift of the ion spectrum and of the plasma lines. If this difference can be measured at three separate receiving stations then it should be possible to determine the true vector of electric current. So far, however, this is only a theoretical proposal and no measurements of this kind have yet been published (Bauer *et al* 1976).

5. Parameters derived from IS measurements

From the list of parameters measured directly, several others can be estimated, including the static electric field; the Hall and Pedersen conductivities and hence the electric current perpendicular to the magnetic-field lines; the wind speed and temperature of the neutral atmosphere; and the downward flux of heat from the exosphere.

5.1. Electric field, E

In the F region of the ionosphere, the magnitudes of the gyro-frequencies of both ions (ω_{iB}) and electrons (ω_{eB}) are far greater than the corresponding collision

frequencies (ν_{in} and ν_{en}). As a result both ions and electrons tend to spiral *along* the magnetic-field lines, except in the presence of an electric field which causes the ions and electrons to drift *across* the magnetic-field lines with a velocity of $\boldsymbol{V}_\perp = \boldsymbol{E} \wedge \boldsymbol{B}/B^2$ where $\boldsymbol{B}$ is the magnetic induction.

If, therefore, $\boldsymbol{B}$ is known—as is usually the case—measurements of the total vector of drift velocity can be used to determine $\boldsymbol{E}_\perp$, the electric field in a plane perpendicular to the magnetic-field lines. In the F region at mid-latitudes it can be assumed that the magnetic-field lines carry charged particles so easily that no permanent electric field can be sustained along the field line, in which case $\boldsymbol{E} = \boldsymbol{E}_\perp$.

Two mechanisms are now thought to be responsible for the electric fields observed in the ionosphere. In the E region, neutral winds tend to separate ions from electrons, thus generating electric fields by the dynamo mechanism, and these fields can be 'mapped' upwards into the F region by the highly conducting magnetic-field lines. At the same time it is thought that a connection is established between the Earth's magnetic field and the magnetic field carried through interplanetary space by the solar wind. As a consequence, the high-latitude field lines are swept over the poles, so generating a magnetospheric electric field which is 'mapped' downwards into the F region at high and mid latitudes, especially during auroral magnetic disturbances (Banks and Doupnik 1975).

Figures 18(*a*) and (*b*) show electric fields measured by the IS system at Malvern, UK during magnetically quiet and disturbed days respectively.

5.2. Ionospheric conductivities, σ_H and σ_P

As described above, the main effect of an electric field in the F region of the ionosphere is to move the plasma as a whole perpendicular to the magnetic-field lines. At lower heights, however, collisions with the neutral atmosphere affect the movement of charged particles. As a result the mean velocities of the ions and electrons under the influence of an electric field are slightly different, and this corresponds to an electric current.

For an electric field applied perpendicular to the magnetic field, the current induced in a direction perpendicular to both is governed by the Hall conductivity:

$$\sigma_H = (Ne/B)[\omega_{iB}^2(\nu_{in}^2 + \omega_{iB}^2)^{-1} - \omega_{eB}^2(\nu_{en}^2 + \omega_{eB}^2)^{-1}]$$

while the current induced in a direction parallel to the applied electric field is governed by the Pedersen conductivity:

$$\sigma_P = (Ne/B)[\nu_{in}\omega_{iB}(\nu_{in}^2 + \omega_{iB}^2)^{-1} + \nu_{en}\omega_{eB}(\nu_{en}^2 + \omega_{eB}^2)^{-1}].$$

In the height range 105–140 km, $\omega_{iB} \ll \nu_{in}$ and $\omega_{eB} \gg \nu_{en}$ so that

$$\sigma_H \simeq Ne/B$$

and

$$\sigma_P \simeq (Ne/B)[\nu_{in}\omega_{iB}(\nu_{in}^2 + \omega_{iB}^2)^{-1}].$$

Above about 150 km, both conductivities fall sharply to zero. Knowing the magnetic-field strength and the ion composition at each height, ω_{iB} can be calculated, while direct IS measurements of N and ν_{in} can be made. In this way both σ_H and σ_P can be determined for all heights above about 105 km. If $\boldsymbol{E}_\perp$ is also known, the currents flowing perpendicular to the magnetic-field lines (and the resultant Joule

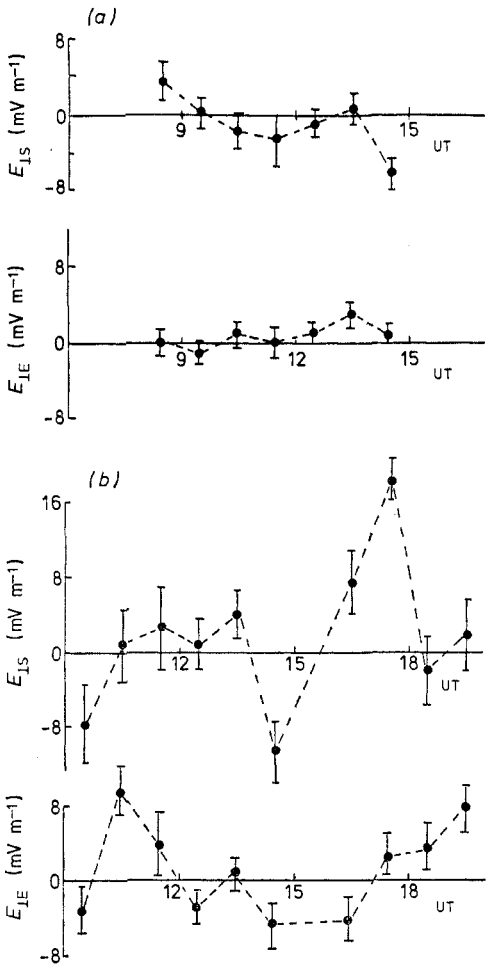

Figure 18. Electric fields 265 km above Malvern on (*a*) a quiet day and (*b*) a disturbed day.

heating) can be estimated. Such measurements have been made successfully at Chatanika in the auroral zone where strong currents are frequently observed (figure 19).

5.3. Neutral wind velocity, V_n

In the E region of the ionosphere, the ion–neutral collision frequency is much greater than the gyro-frequency. As a result, the presence of the Earth's magnetic field can be effectively ignored when the movement of the ion population is considered, and it can be assumed that the ions have the same mean velocity as the neutral atmosphere. A measurement of the true vector of ion drift velocity, based on the Doppler shift of the ion spectrum of the scattered signal, then gives the neutral wind velocity vector directly. Thus for heights below ~ 120 km where $V_n = V_p$ both the meridional and zonal components of the neutral wind can be determined (Evans 1972).

At F-region heights the situation is more complicated. Here the gyro-frequencies

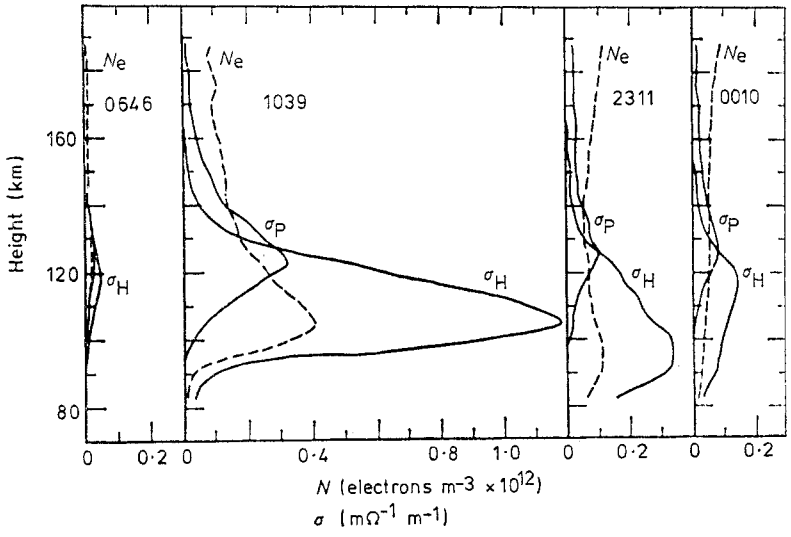

Figure 19. Altitude profiles for N, σ_H and σ_P for four separate universal times, 13–14 October 1972 measured at Chatanika (from Banks and Doupnik 1975).

for both ions and electrons are far greater than the corresponding collision frequencies and the plasma is constrained to move along the magnetic-field lines. In general the plasma moves under the influence of a number of factors such as winds in the neutral atmosphere, ambipolar diffusion due to gradients in plasma pressure, gravity, electric fields, and the total velocity of the plasma along the field lines is given by:

$$V_{\parallel} = u_x \cos I + \sin I\{\partial[Nk(T_i + T_e)]\partial h + Nm_i g\}/Nm_i \nu_{in} + V_{\perp} \cot I$$

where u_x is the meridional component of the neutral wind and $V_{\perp}$ is the plasma velocity perpendicular to the magnetic-field lines in the meridian.

Using the technique of incoherent scatter $V_{\parallel}$, $V_{\perp}$, N, m_i, T_i and T_e can be measured as functions of h, and ν_{in} estimated, so that u_x, the neutral wind velocity in the meridian, can be obtained (figure 20). Unfortunately the plasma in the F region does not respond to a neutral wind perpendicular to the field lines so the zonal wind cannot be measured.

5.4. Neutral temperature, T_n

In the E region of the ionosphere the ion–neutral collision frequency is so great that the ions would be expected to be at the same temperature as the neutral constituents, and this has indeed been confirmed by *in situ* measurements. Hence for E-region heights incoherent-scatter measurements of the ion temperature give the neutral temperature directly together with the ion–neutral collision frequency (see §4.6 and figure 16).

In the F region, the ion–neutral collision frequency is smaller and as a result T_i may typically be expected to be 50–100 K higher than T_n. At these heights, the temperature of the ions is maintained in a steady state by the balance between a heat input from elastic collisions with free electrons, and a heat loss from elastic

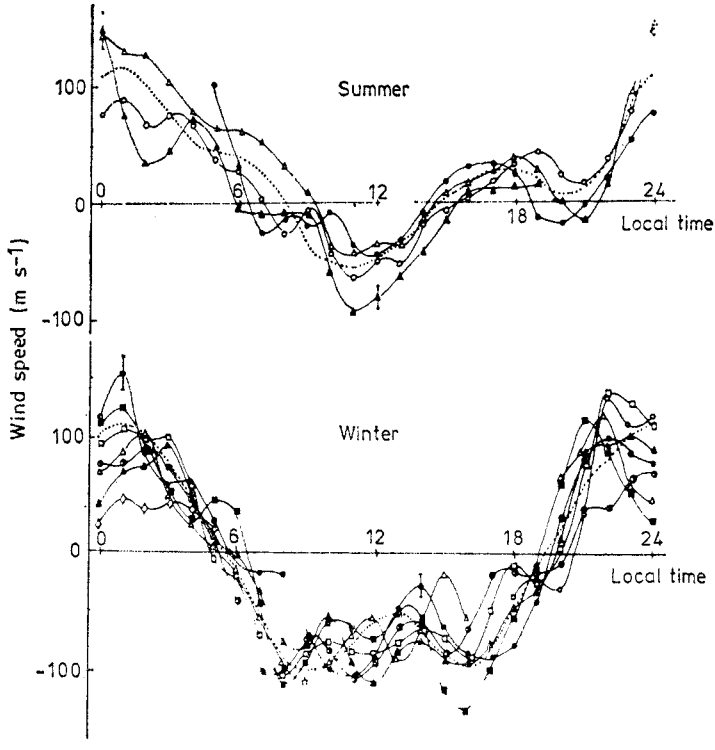

Figure 20. Neutral meridional wind at 300 km at St Santin (from P Amayenc 1975, private communication). Summer: 6–9 July 1971; winter: 25 January–1 February 1972. Dotted curves are mean values.

collisions with neutral atoms and molecules, and from 'charge-exchange' collision processes.

Near the peak of the F2 layer the dominant ion is O^+ and the principal neutral constituent is N_2 and at this height it can be shown that:

$$T_n = T_i - N(T_e - T_i)T_e^{-3/2}[4{\cdot}4\times10^{-9}(T_i+T_n)^{1/2}n(O)+1{\cdot}4\times10^{-7}n(N_2)]^{-1}$$

where N, $n(O)$ and $n(N_2)$ refer to number densities of electrons, atomic oxygen and molecular nitrogen respectively.

Incoherent-scatter measurements of T_e, T_i and N combined with data on $n(O)$ and $n(N_2)$ for model atmospheres (CIRA 1972) can be used in the above expression to deduce values of T_n. Above about 300 km the neutral atmosphere has a high thermal conductivity and T_n only shows a slight increase with height as it tends to its limiting value, the so-called exospheric temperature. In figure 21 measurements of exospheric temperature by the IS technique are compared with values deduced from a satellite experiment (Thuillier *et al* 1977).

5.5. Downward flux of heat from the exosphere, Φ

For a population of electrons in a gas of singly charged ions it can be shown that the thermal conductivity of the electrons is given by:

$$K_e = 1{\cdot}23\times10^{-11}\,T_e^{5/2} \qquad \mathrm{J\ m^{-1}\ s^{-1}\ K^{-1}}$$

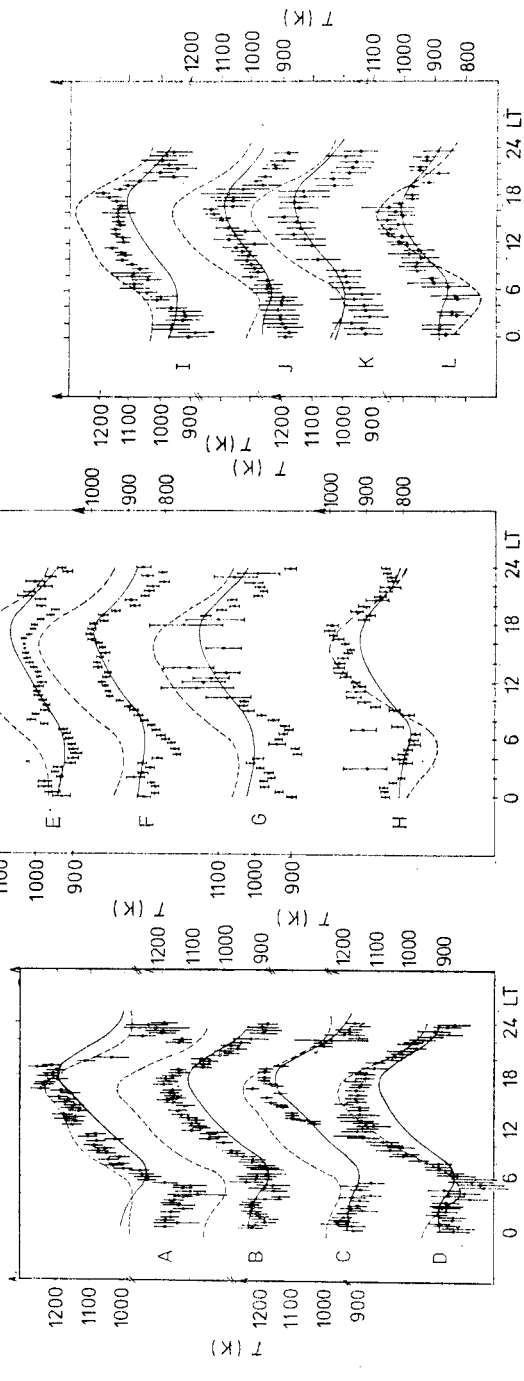

Figure 21. Diurnal variation of exospheric temperature for different seasons from satellite observations and from three incoherent-scatter stations. (*a*) Arecibo, (*b*) St Santin, (*c*) Millstone Hill. ———, predicted variation based on spectral profile of the 630 nm airglow line (OGO-6) (from Thuillier *et al* 1977); — — —, predicted variation based on mass spectrometer data from four satellites (from Hedin *et al* 1974). A: 26 June 1968, B: 24–25 September 1968, C: 11–12 April 1968, D: 17–28 December 1968, E: 8 July 1971, F: 24 September 1971, G: 14 April 1971, H: 15 December 1971, I: 18–19 July 1970, J: 28–29 September 1970, K: 23–24 March 1970, L: 28–29 December 1970.

while the thermal conductivity of the ions of mass number M_i:

$$K_i = 7{\cdot}4 \times 10^{-13} M_i^{-1/2} T_i^{5/2} \qquad \text{J m}^{-1}\,\text{s}^{-1}\,\text{K}^{-1}.$$

For all heights between 250 and 600 km, O^+ is the dominant ion so that $M_i = 16$ and

$$K_i = 1{\cdot}85 \times 10^{-13} T_i^{5/2} \qquad \text{J m}^{-1}\,\text{s}^{-1}\,\text{K}^{-1}.$$

It follows that almost all the downward flux of heat in the top-side of the ionosphere is carried by electrons, and as free electrons are usually constrained to travel along the magnetic-field lines, the heat flux in this direction:

$$\Phi = -K_e \sin I\, \partial T_e/\partial h$$
$$= -1{\cdot}23 \times 10^{-11} \sin I\, T_e^{5/2}\, \partial T_e/\partial h \qquad \text{J m}^{-2}\,\text{s}^{-1}.$$

This conduction of heat downwards from the top-side ionosphere is an important factor in determining the total energy balance in the various ionospheric layers, and if the height profile of electron temperature can be accurately measured using the IS technique, then the flux of heat can be determined. For example, Bauer *et al* (1970) used data from the French IS facility to study the thermal coupling between the upper F2 region and the magnetosphere.

6. Method of observation

In using IS to derive accurate profiles of different parameters we need to define the altitude from which a particular scattered signal comes. This can be done in two ways.

(i) A short pulse can be transmitted and the range of the scattering medium can be determined by the time delay between transmission and reception. Because the frequencies used in IS are so much higher than the plasma frequencies encountered in the atmosphere we can assume that the radar signal travels at c, the velocity of light *in vacuo*, and there is no difference between virtual height and real height as there is for an ionosonde signal.

(ii) A continuous-wave signal is transmitted vertically upwards by one aerial, and the scattered signal is received by a second aerial at a suitable distance so that the altitude is defined by the intersection of the two beams.

The pulsed radar is the method that has been most commonly used. It requires only one antenna and is often referred to as the monostatic method. When CW radar is used with two or more separate aerials it is referred to as bistatic or multistatic, respectively.

6.1. Monostatic system

Let a peak power, LP_p, be transmitted by an aerial for a pulse length τ, where P_p is the peak power leaving the transmitter and L is a factor representing the loss between the transmitter itself and the feed of the aerial.

If the gain of the transmitting aerial in the direction (θ, ϕ) equals $G(\theta, \phi)$, then the peak power incident per unit area on a volume of plasma at a range R in this direction equals $LP_pG(\theta, \phi)/4\pi R^2$.

Now the total scattering volume occupied by the pulse between zenith angles θ and $\theta+\mathrm{d}\theta$ and between azimuths ϕ and $\phi+\mathrm{d}\phi$ can be written:

$$R\,\mathrm{d}\theta R\sin\theta\,\mathrm{d}\phi c\tau/2.$$

Therefore the scattering cross section of this volume (for $\lambda \gg D$) is given by:

$$R^2\sin\theta\,\mathrm{d}\theta\,\mathrm{d}\phi c\tau N\sigma_e/2(1+T_e/T_i)$$

and the power scattered by this volume, picked up by the aerial and delivered to the receiver, is given by:

$$L^2P_p\lambda^2c\tau G^2(\theta,\phi)\sin\theta\,\mathrm{d}\theta\,\mathrm{d}\phi N\sigma_e/128\,\pi^3R^2(1+T_e/T_i)$$

(where we assume that the loss between transmitter and feed is equal to the loss between feed and receiver and that γ, the angle between the direction of the incident electric field and the direction to the observer, is 90° for direct back-scatter).

The power scattered back to the receiver is then given by:

$$L^2P_p\lambda^2c\tau N\sigma_e\int_0^{\pi/2}\int_0^{2\pi}G^2(\theta,\phi)\sin\theta\,\mathrm{d}\theta\,\mathrm{d}\phi/128\,\pi^3R^2(1+T_e/T_i).$$

For a square aperture, uniformly illuminated:

$$\int_0^{\pi/2}\int_0^{2\pi}G^2(\theta,\phi)\sin\theta\,\mathrm{d}\theta\,\mathrm{d}\phi=0{\cdot}89\times2\pi G(0,0)$$

and for a parabolic dish, illuminated by the feed so that there is a 10 dB taper between the centre and edge of the dish, the same integral equals $0{\cdot}76\times2\pi G(0,0)$ ($G(0,0)$ is the maximum gain of the aerial and equals $4\pi A_c/\lambda^2$ where A_c is the effective collecting area of the aerial).

The instantaneous power scattered back from the pulse to the receiver (P_s) is therefore given by

$$P_s\simeq5{\cdot}3\times10^{-22}L^2P_p\tau A_cN/R^2(1+T_e/T_i).$$

This power is spread over a bandwidth B which, for $T_e/T_i<4$, is approximately equal to $14(kT_i/m_i)^{1/2}/\lambda$ (see figure 7).

In addition, there is an average noise power (P_n) over this bandwidth which is represented by an equivalent system-noise temperature (T_s) so that $P_n=kT_sB$. This system noise is made up of background noise radiated from the sky, especially synchrotron radiation from the Galaxy (represented by T_{sky}), thermal noise from loss in the feed between the aerial and the amplifier input $[(1-L)T_{amb}]$ and the input noise of the pre-amplifier (T_{preamp}) so that at the pre-amplifier:

$$P_n=kT_sB=k[LT_{sky}+(1-L)T_{amb}+T_{preamp}]B$$

and the average instantaneous power over the bandwidth while scattered signals from the pulse are being received equals (P_s+P_n).

Due to the random nature of both the scattered signal and the noise, this instantaneous power is constantly fluctuating, but if the signal received from a given height over a period of t seconds is averaged, then the total effective integration time will be $p\tau t$, p being the pulse recurrence rate. If at the same time the observed spectrum is smoothed over a bandwidth b, then the uncertainty in the average power measured for any part of the spectrum is given by

$$\delta P\approx(P_s+P_n)b[(p\tau tb)^{1/2}B]^{-1}$$

while the signal power for the same part of the spectrum $\approx P_sb/B$.

The signal-to-noise ratio is thus approximately

$$P_s b/\delta PB = (p\tau tb)^{1/2} P_s/(P_s + P_n).$$

For $P_s \gg P_n$ (which is the case when a very powerful radar system is observing the daytime F region), the signal-to-noise ratio equals $(p\tau tb)^{1/2}$.

For $P_s \ll P_n$ (which is the case for a less powerful system or when the same system is observing the D region, or the top-side ionosphere) the signal-to-noise ratio after inserting numerical values for c, σ_e and k is approximately:

$$40L^2 P_p (p\tau^3 tb)^{1/2} A_c N[T_s B(1 + T_e/T_i)R^2]^{-1}.$$

Hence, for high-resolution observations over the maximum possible height range, the collecting area of the aerial should be as large as possible, the losses in the aerial feed and the system noise should be kept to a minimum, and B should be reduced until it just covers the ion spectrum of the scattered signal.

For the other variable parameters, however, the optimum values are not so obvious. For example, b should not be so large that real spectral information is smoothed out, neither should t be so large that it masks real temporal change in the ionosphere; p should not be increased to such an extent that the scattered signal from a lower height is confused by the signal from an earlier pulse scattered from a greater height.

P_p is limited by the design of the transmitter, but so is the maximum average power transmitted (P_{av}) which equals $P_p \tau p$. In fact, for $P_s \ll P_n$ the signal-to-noise ratio is proportional to $(P_{av} \tau^{1/2} p^{-1/2})$ which suggests that τ should be made as *long* as possible, reducing p at the same time to keep $p\tau$ constant.

There is a second reason why the pulse length, τ, should be as *long* as possible. If τ is too small, then the half-power bandwidth of the transmitted signal (which equals $0{\cdot}89\ \tau^{-1}$) will be increased until it is comparable with the bandwidth of the spectrum of the scattered signal, B, and if this occurs all detailed spectral information will be lost.

However, there is a counter-argument for keeping τ as *short* as possible. Figure 22 shows that the minimum height resolution obtained with a pulse of length τ is $\frac{1}{2}c\tau$, and if the scattered signal has been gated at the receiver, in time intervals of τ_g, then the signal received in each gate might have been scattered from a total height range of $\frac{1}{2}c(\tau + \tau_g)$.

For several of the early IS systems, this conflict between long pulses and short pulses was a fundamental limitation. Long pulses gave good signal-to-noise performance and fine spectral resolution, but poor height resolution. Short pulses gave a good height resolution but poor signal-to-noise and poor spectra.

These conflicts have now been resolved by using more sophisticated radar techniques. For example, Farley (1969, 1972) has shown that good height resolution can be reconciled with good spectral resolution if a group of short pulses (i.e. short enough to give good height resolution) are set at variable spacings within an envelope long enough to give good spectral information. For example, if we transmit pulses of length τ at times 0, τ', $4\tau'$, and $6\tau'$ ($\tau < \tau'$) then we can measure the autocorrelation function of the scattered signal from a given height for time lags of 0, τ', $2\tau'$, $3\tau'$, $4\tau'$, $5\tau'$ and $6\tau'$, so providing all the spectral information of a pulse of length $6\tau'$ while retaining the height resolution corresponding to τ (figure 23). Similarly, multiple pulses transmitted at times 0, τ', $8\tau'$, $11\tau'$, $13\tau'$ and $17\tau'$ give 15 of the 17 lags present in the autocorrelation function of a single pulse of length $17\tau'$.

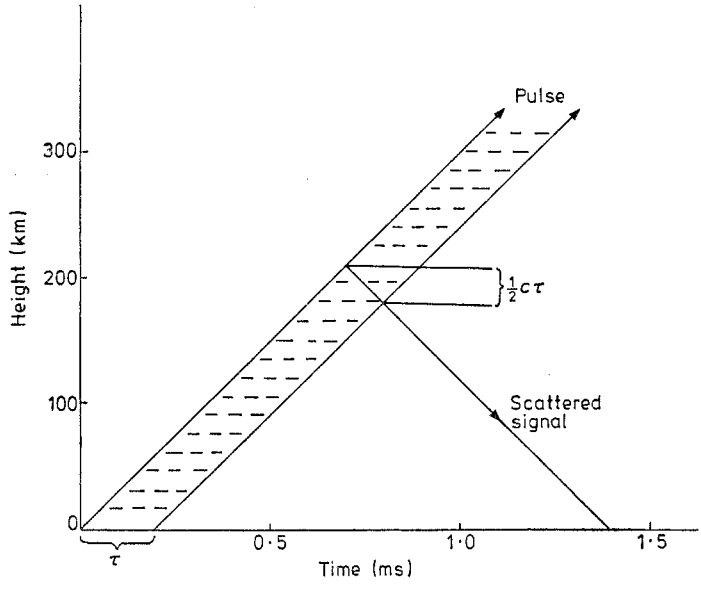

Figure 22. Scattering of a single pulse for a monostatic system with a height resolution of $\frac{1}{2}c\tau$.

Using such multi-pulse techniques it has proved possible to obtain totally adequate spectral resolution, and by reducing the length of the individual pulses, the height resolution can be improved. If τ is reduced too much, however, the signal-to-noise ratio eventually becomes inadequate. To improve height resolution still further while retaining an adequate signal-to-noise ratio each pulse can be split into a number

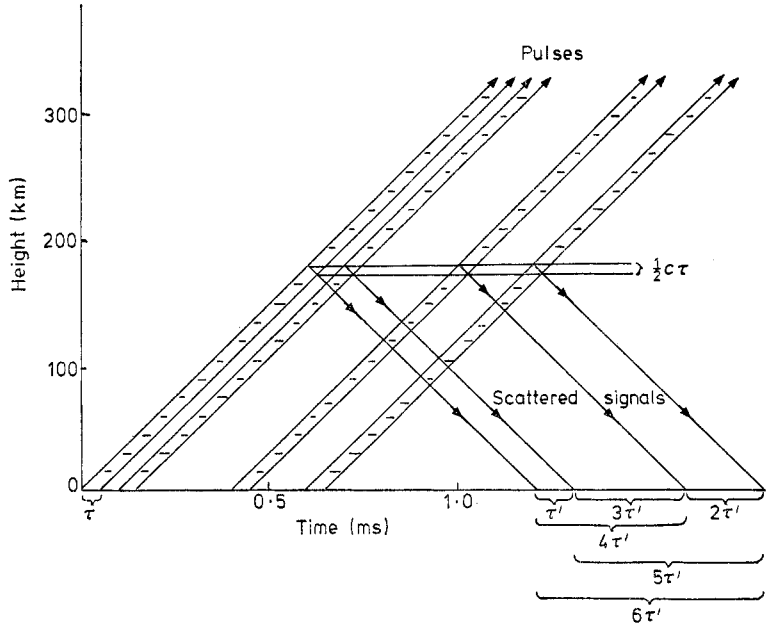

Figure 23. Scattering of multiple pulses of variable spacing.

of subpulses with the option of changing the phase of the transmitted signal by 180° at the beginning of each subpulse. The use of this phase-change option is determined by a series of codes devised by Barker (1958), and if the receiver is coded in the same way a considerable improvement in effective height resolution is achieved without sacrificing the signal-to-noise ratio to the extent necessary if extremely short pulses were used.

Figure 24 illustrates the simplest example of a three-bit code (+ + −). Using a similar code in the receiver we see that the scattered signals almost completely cancel out for all heights except one. Other known Barker codes are four-bit (+ + − +); five-bit (+ + + − +); seven-bit (+ + + − − + −); eleven-bit (+ + + − − − + − − + −) and thirteen-bit (+ + + + + − − + + − + − +). Gray and Farley (1973) have given a full account of the use of phase-reversal codes in incoherent-scatter measurements.

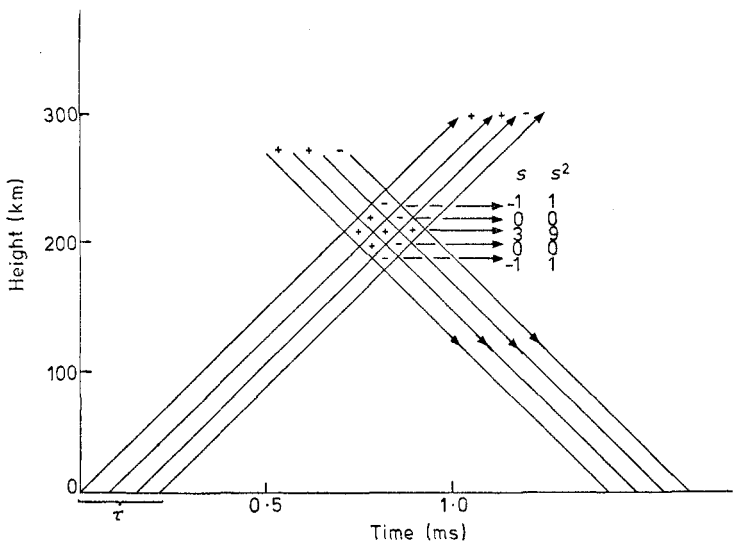

Figure 24. Barker coding of a single pulse to achieve better height resolution. (For clarity a longer pulse is shown than would normally be used for Barker coding.)

Using sophisticated techniques such as these, many of the limitations of early monostatic IS systems can be overcome. One limitation remains—a monostatic system can only measure plasma drift velocity in a single direction at a given time. If the antenna is steerable, it is possible to scan a cone of directions, and if it can be assumed that the drift velocity is constant over the time taken to complete the scan and over the horizontal distances covered by the cone, then the total vector of drift velocity can be estimated. To measure the true drift velocity of a single volume of plasma, however, a multistatic radar system must be used.

6.2. Multistatic system

In a multistatic system height resolution is achieved by the intersection of two beams. Let the beams intersect at a distance R_1 from the transmitting aerial and R_2 from the receiving aerial, as shown in figure 25. For simplicity it is assumed that the transmitting aerial points vertically upwards and has a cylindrically sym-

metrical beam with a half-power beamwidth of θ_1. This beam is intersected by the beam of the receiving aerial over a vertical range of $R_2\theta_2/\cos\chi$, where χ is the elevation of the beam and θ_2 is the half-power beamwidth in elevation.

The scattering cross section of the intersecting volume is then given by:

$$\pi(R,\, \theta_1/2)^2 R_2\theta_2 N\sigma_e\langle\sin^2\gamma\rangle/\cos\chi(1+T_e/T_i)$$

and for a circularly polarised transmitted beam $\langle\sin^2\gamma\rangle=(1-\cos^2\chi/2)$. If a CW wave of power LP_{av} is transmitted, and if the azimuth beamwidth of the receiving aerial (ϕ_2) completely covers the transmitted beam (i.e. if $R_2\phi_2 > R_1\theta_1$), then it can be shown that the power scattered to aerial 2 and delivered to the receiver (P_s) is given by:

$$LL'P_{av}\lambda d_2 N\sigma_e(1-\cos^2\chi/2)[16R(1+T_e/T_i)]^{-1}$$

(where d_2 is the effective diameter of the receiving aerial corresponding to the azimuth beamwidth ϕ_2, R is the horizontal distance between the transmitter and the receiver and L' is the loss factor for the receiver aerial).

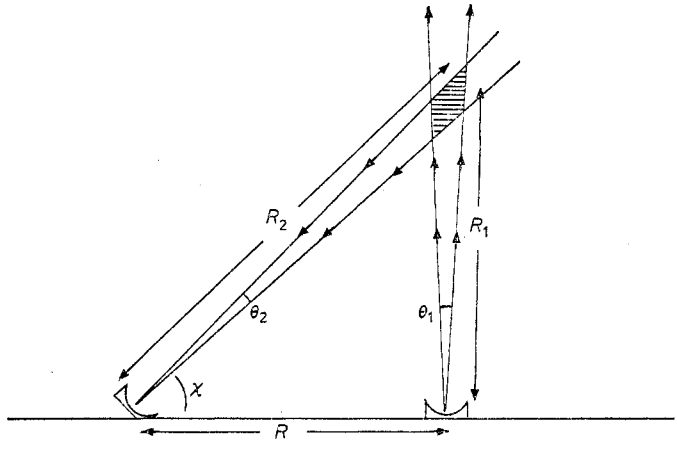

Figure 25. Bistatic incoherent-scatter system.

After averaging the received signal for a time t and smoothing the spectrum over a bandwidth b, the final signal-to-noise ratio at this point in the spectrum $\simeq(bt)^{1/2}P_s(P_s+P_n)^{-1}$.

For $P_s \gg P_n$, the signal-to-noise ratio corresponds entirely to 'self-noise' and equals $(bt)^{1/2}$. For $P_s \ll P_n$, on the other hand, it is the system noise that is all-important and in this case the final signal-to-noise ratio is given by:

$$LL'P_{av}\lambda d_2(bt)^{1/2}N\sigma_e(1-\cos^2\chi/2)[16\,RkT_sB(1+T_e/T_i)]^{-1}.$$

For maximum signal-to-noise ratio it is clear that P_{av} should be as large as possible, and the losses in the feed and the system noise should be as small as possible.

However, the signal-to-noise ratio does not depend on the gain of the transmitting aerial, nor on the height of the scattering region (except for the variation of N) nor on the elevation diameter of the receiving aerial. The signal-to-noise ratio is proportional to the effective azimuth diameter of the receiving aerial, but only while $R_2\phi_2 > R_1\theta_1$. If $R_2\phi_2 < R_1\theta_1$, i.e. the horizontal width of the beam of the receiving aerial at the scattering volume is less than the width of the transmitted beam, no

further improvement in signal-to-noise ratio can be achieved by increasing the gain of the receiving aerial.

The ideal dimensions for the two aerials are those for which the two beams 'match' at the scattering volume. Any further improvement in the gain of either aerial improves the resolution of the system, but not the signal-to-noise ratio.

It follows that multistatic observations can be made with relatively small aerials and a simple transmitter. To measure the total vector of plasma drift velocity, however, it is necessary to establish and maintain a transmitting station and three receiving stations. A further disadvantage of a multistatic system is that it only observes one height at a time, although this limitation can be partly offset by scanning or by using multi-beam receiving aerials.

7. Incoherent-scatter facilities

A full IS facility includes a powerful radar transmitter, at least one large antenna, low-noise receivers and sophisticated data-processing equipment. Such a facility is very expensive and up to the present day only a few have been constructed. Table 1 lists the main features of seven systems which have provided a substantial amount of data on the upper atmosphere.

Four of the facilities lie on the American continent, covering a wide range of latitudes between the magnetic equator and the auroral zone.

7.1. Jicamarca

One of the earliest IS facilities, and still one of the most powerful, began observations in 1961 at Jicamarca near Lima, Peru (Bowles 1963). The site was chosen because it lies within 2° of the magnetic equator. This radar is therefore ideally sited to study the equatorial electrojet and to observe vertical plasma movements driven by an east–west electric field. The site also proved favourable for the construction and operation of the facility. It lies in an extremely flat desert area surrounded by the steep foothills of the Andes which help to protect the receiver from radio interference and from stray echoes reflected by mountains at distances of 100 km or more which might otherwise 'clutter' the echoes from the ionosphere.

To take advantage of a flat site, the antenna is composed of a two-dimensional array of simple half-wave dipoles, mounted $0{\cdot}3\lambda$ from the ground and covering a square area 290 m by 290 m. This array is divided into 64 equal modules which are fed by a branching system of coaxial cables. By inserting extra lengths of cable into the feed connected to each module, the antenna beam can be steered away from the zenith by up to 3°. Each module is, in turn, made up of 12 rows of 12 dipoles, all fed in phase. This array thus includes 9216 dipoles.

A second array of dipoles, lying orthogonal to the first, covers the same area of ground and as the two orthogonal polarisations can be fed independently, the antenna is suitable for making polarisation measurements, e.g. measurements of the Faraday rotation of the scattered signal.

In full operation, the transmitter consists of 4 cavity-mounted triodes, each giving about 1 MW peak power. The triodes can be used in parallel, delivering power into a single lead, or they can operate in pairs, with each pair providing a pulse of left- and right-handed circular polarisation in turn.

Table 1.

Station	Location	Dip latitude	Antenna	Frequency (MHz)	Power Peak (MW)	Power Mean (MW)	Mode
Jicamarca (1962–)	11·9 °S 76·9° W	1° N	290 m × 290 m dipole array	49·9	4	0·4	Vertical, pulsed
Arecibo (1962–)	18·3° N 66·8° W	30° N	305 m spherical reflector	430·0	2	0·1	Vertical, pulsed
Millstone Hill (1963–)	42·6° N 71·5° W	57° N	68 m parabola	440·0	3	0·12	Vertical, pulsed
			25 m parabola	1295·0	4	0·12	Oblique, pulsed
Stanford (1965–71)	37·4° N 122·2° W	43° N	27 m parabola	1300·0	5	0·12	Oblique, pulsed
Chatanika (1971–)	64·9° N 147·7° W	65° N	27 m parabola	1300·0	5	0·12	Oblique, pulsed
Kharkov (1972–)	48·5° N 36° E		100 m parabola	150	2		Vertical, pulsed
St Santin (1965–)	44·6° N 2·2° E	41° N	20 m × 100 m reflector	935		0·15	Vertical cw
Nancay (1965–)	47·4° N 2·2° E		40 m × 200 m reflector	Receiving stations			
St Cassien (1973–)	44·7° N 0·8° E		25 m parabola				
Mende (1973–)	44·5° N 3·5° E		25 m parabola				
Malvern (1968–75)	52·1° N 2·3° W	50° N	43 m parabola	400·5	8	0·08	Vertical, pulsed
				400·5		0·04	Vertical cw
Wardle (1971–75)	53·1° N 2·6° W		25 m × 36 m parabola	Receiving stations			
Chilbolton (1971–75)	51·1° N 1·4° W		25 m parabola				
Aberystwyth (1972–75)	52·4° N 4·0° W		Two 12 m × 25 m parabolic troughs				

When the Jicamarca radar was first planned it was hoped that it would measure the ion-gyro-resonance effect—a predicted modulation in the ion spectrum caused by the gyro-resonance of the ions. For this to be possible it was recommended that the wavelength used should equal the gyro-radius of the ions, and so a wavelength of 6 m was chosen. Such a long wavelength made the construction of the dipole array much simpler and it also had the advantage of making the facility very suitable for the Faraday rotation method of measuring the electron density profile, because the total rotation of the polarised signal varies as λ^2.

However, there are two major disadvantages in using such a long wavelength. In the first place, the antenna receives synchrotron radiation from the Galaxy, and at 49·9 MHz this is equivalent to a minimum system noise temperature of 6000 K

which severely limits the sensitivity of the radar. Secondly, when such a wavelength is used in a direction perpendicular to the magnetic-field lines, the results will suffer from coherent scatter from small-scale irregularities in electron density. However, in recent years, the comparatively long wavelength of the Jicamarca instrument has been turned to advantage by using coherent echoes to measure wind velocities in the stratosphere (15–35 km) and the mesosphere (60–85 km) (Rastogi and Bowhill 1975) and to study the equatorial electrojet and spread-F irregularities (see §8.3).

7.2. Arecibo

The most sensitive and most sophisticated IS facility in use at present is at Arecibo in Puerto Rico (Gordon 1964). This began operation in 1962 and as was the case in Jicamarca, the antenna was designed to take full advantage of a suitable site. A limestone sink-hole of roughly the right shape and size was chosen and the surface shaped to give an approximately spherical section. A mesh-wire reflecting surface was then supported on posts to give an exact spherical section with a radius of curvature of 245 m and an aperture diameter of 305 m. Since the reflecting surface is spherical, a parallel beam is brought to a line focus and so a carefully designed line feed is used to illuminate the dish. This feed is supported from a platform which in turn is supported above the focal line by cables which pass over the top of three towers spaced around the circumference of the dish.

Because the reflector is spherical it is possible to scan the beam as far as 20° from the zenith by moving the feed along an arc of a circle with the same radius of curvature as the reflector itself, thus maintaining an almost identical geometrical relationship between the feed and the reflector. The ability of the system to scan rapidly in a 20° cone about the zenith has proved important in measuring plasma velocities in different directions so that the true vector of plasma drift can be estimated.

The pre-eminence of Arecibo, however, is based on its sensitivity which allows it to make accurate measurements over a very large height range. The actual transmitter used at Arecibo is less powerful than the original transmitter at Jicamarca and the effective collecting area of the antenna is less than that of the Jicamarca array, but the system noise temperature at Arecibo is far smaller. Arecibo operates at a frequency of 430·0 MHz and at this frequency the noise temperature of unavoidable galactic radiation is, on average, less than 40 K so that by using a low-noise pre-amplifier the overall system noise can be kept very low. At this frequency, coherent scattering is also far less of a problem, and as a result the Arecibo instrument has been able to measure electron densities over a height range from 80 km to 4500 km (see §8.4).

The high sensitivity of the Arecibo instrument also allows the use of sophisticated pulse patterns that sacrifice signal-to-noise ratio in return for improved height resolution. It was at Arecibo that both the multiple-pulse technique and the Barker coding of subpulses were pioneered. For example, using five- and seven-pulse groups, Zamlutti and Farley (1975) made measurements of the E region with a height resolution ranging from 1 to 3 km without significant smoothing of spectral detail. Furthermore, Ioannidis and Farley (1972, 1974) have used three- and thirteen-baud Barker coding of single pulses to study the D and E regions, including the sporadic-E layer, with a height resolution of 900 m.

The high sensitivity of the Arecibo facility has also permitted observation of the

plasma lines for the study of both electron density profiles and the incident flux of suprathermal electrons. Recently plasma line observations have been combined with the transmission of HF radio signals at the plasma frequency which can enhance the strength of the 'plasma' lines by a factor of 10^4 (Gordon and Carlson 1974).

7.3. Millstone Hill

The choice of operating frequency for an IS facility always presents a difficulty. If the frequency is too low the signal is contaminated by coherent echoes from ionospheric irregularities such as spread-F, and the background system noise is unavoidably high due to synchrotron radiation from the Galaxy. If, however, the wavelength is too short compared with the Debye length no useful measurements can be made.

The IS facility at Millstone Hill, near Boston, resolves this dilemma by using two radar systems operating at wavelengths of 68 cm and 23 cm respectively. The use of two systems also resolves the dilemma in antenna design between sensitivity and steerability. At 68 cm, the antenna used is a fixed parabola, 68 m in diameter and pointing vertically upwards, while at 23 cm a fully steerable 25 m parabola is used.

The fixed antenna has the greater sensitivity and is used for measuring electron density, and electron and ion temperature up to a height of 2000 km. Normally a single-pulse mode is employed with pulse lengths of 100, 500 and 1000 s. By using all three pulse lengths it is possible to obtain $N(h)$ from 100 to 2000 km, while T_e and T_i can be determined in the range 225–1125 km but only with a height resolution of about 75 km. In order to achieve an improved height resolution without sacrificing the measurements of T_e and T_i a 'two-pulse' mode is used and this gives T_e and T_i with height resolution of 6 km between 120 and 165 km, and 15 km between 165 and 315 km.

The fixed antenna is also able to measure plasma drift velocity in the vertical direction, but is unable to measure horizontal components. To measure these, the 25 m steerable parabola is used. Directed northwards at an elevation of 18° this antenna measures the meridional velocity perpendicular to the Earth's magnetic field, while observations westward give the zonal component velocity. If it is assumed that there are no major variations in the velocity components during the 48 min required to measure the meridional and zonal components, and that the drift motion is uniform between the different scattering volumes, then the three-dimensional drift velocity can be obtained (Carpenter and Kirchhoff 1974). Using this technique, tidal motions in the E region have been observed (Evans 1972) and F-region velocities perpendicular to $\boldsymbol{B}$ have been compared with simultaneous observations at high latitudes to study the penetration of magnetospheric electric fields to mid-latitudes (Carpenter and Kirchhoff 1975).

The Millstone Hill system began measurements in 1963 and has since maintained a regular observing schedule of two days a month. Data on F-region electron density, electric and ion temperature and vertical drift velocity based on these routine measurements have now been regularly published over a sunspot cycle and represent a major contribution to upper-atmosphere studies.

A serious problem for any large IS system operating on a routine basis is the sheer volume of data produced. For example, in the Millstone Hill 'one-pulse' measurements some 11 000 separate data points are produced in a single 24 h run.

The routine computer analysis of the data is handled in three stages: (i) all data points are automatically examined and those which are clearly unreliable are rejected, (ii) a series of orthogonal polynomials are fitted to the remaining points to give the profile with the best overall least-squares fit, (iii) contour paths are then plotted to represent these profiles. Samples of data published at Millstone Hill are illustrated in figure 11.

7.4. Chatanika

Most existing IS systems operate at low or middle latitudes. At such latitudes the lines of magnetic force are 'closed' even at high altitudes and the ionosphere is relatively less influenced by interaction between the magnetic field and the solar wind.

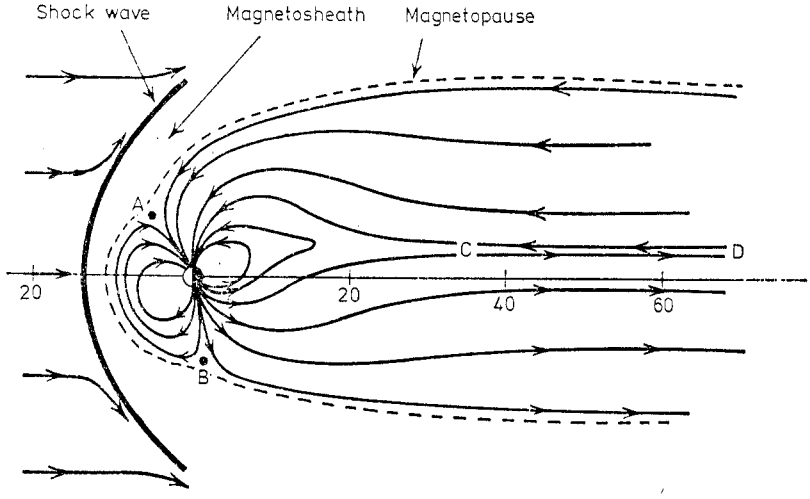

Figure 26. Geomagnetic field lines distorted by the solar wind. A and B are neutral points, and C and D show the neutral sheet. Distances are in units of Earth radii (after Ratcliffe 1972).

At high latitudes, on the other hand, the magnetic-field lines are strongly affected by the solar wind. On the dayside the magnetic-field lines of the Earth connect with those in the interplanetary medium and are then swept back over the poles and drawn out to form a 'magnetotail' (figure 26). These field lines are described as 'open' and many of the important phenomena of the upper atmosphere are the result of interaction with the interplanetary medium along these open field lines. For example, the 'convection' of the field lines over the poles generates a strong magnetospheric electric field which can be observed at high latitudes. Moreover, the polar cap region is open to bombardment by energetic particles from the Sun or the magnetotail and conversely particles from the polar ionosphere can diffuse outwards along the field lines—the so-called 'polar wind'. Observations at high latitude clearly have a vital role to play in any study of these interactions and especially important are observations in the auroral zones near the boundary between 'open' and 'closed' magnetic-field lines.

In 1971, as a pilot project to investigate the possibility of IS studies in the auroral zone, the radar system which had been operating for some years at Stanford, Cali-

fornia, was moved to Chatanika, Alaska (latitude 64·9° N, longitude 147·7° W). The Chatanika system operates in the monostatic mode using a steerable 27 m parabolic dish at a frequency of 1300 MHz. The peak power used is about 5 MW and the pulse lengths range from 10 μs to 500 μs (Leadabrand *et al* 1972). The short pulses are used to provide electron density profiles in the E region and the longer pulses to measure electron density and electron and ion temperatures in the F region. Ionospheric conditions in the auroral zone frequently change very rapidly and detailed study of such changes calls for IS equipment of high sensitivity so that integration times can be kept to a minimum. Furthermore, the drift velocity changes suddenly in both space and time so it is difficult to make satisfactory estimates of the total vector of plasma drift velocity with a monostatic system.

Nevertheless, despite its relatively modest features, the Chatanika facility has already proved highly successful in studying the many problems of the auroral ionosphere, including magnetospheric electric fields; ionospheric currents and related Joule heating and magnetic activity; morphology of the auroral ionosphere and the plasma trough; D-region absorption; the auroral E layer; spread-F irregularities; particle precipitation (including photoelectron flux from the magnetic conjugate point in the southern hemisphere); and magnetic storm effects. The data already obtained at Chatanika have proved conclusively the scientific importance of IS observations in the auroral zone.

The Chatanika radar completes the chain of IS facilities on the American continent. Two IS facilities have also been established in Western Europe.

7.5. Malvern

The first regular IS observations in the UK were made in 1968 at the Royal Radar Establishment, Malvern (Hey *et al* 1968). At first the system operated monostatically using a fixed circular paraboloid 42·7 m in diameter pointing vertically upwards. The transmitter frequency was 400·5 MHz with a peak power of about 8 MW. Most observations were made with a pulse length of 200 μs which gave a height resolution of 30 km and provided profiles of electron density between 100–1000 km at intervals of about 5 min and profiles of T_e and T_i between 200–600 km at intervals of about 30 min. For better height resolution—especially necessary in the E region—pulse lengths of 67 μs and 33 μs were used, but for these observations the bandwidth of the transmitted signal was too wide for useful temperature measurements to be made.

Observations in the monostatic mode continued until 1974, but they were subject to two severe limitations. The design of the transmitter modulator did not allow the use of multiple or coded pulses and so the accuracy of temperature measurements was limited. Secondly the fixed monostatic system could not provide adequate velocity data.

To overcome these limitations, a multistatic system was established in 1971 with a 40 kW continuous-wave signal transmitted from Malvern, and the scattered signal received at 3 receiving sites remote from Malvern. Fortunately, two suitable receiving aerials already existed. In Wardle, the Jodrell Bank Mark III telescope provided a fully steerable aerial with an ellipsoidal aperture 25 m × 36 m and the second aerial was at Chilbolton, an outstation of the Science Research Council Appleton Laboratory. This aerial was also fully steerable with a circular aperture 25 m in diameter. The third receiving aerial near Aberystwyth consisted of two

parabolic troughs, each 12 m × 25 m, connected together to form a single aperture steerable in elevation (Williams and Taylor 1974).

The first true ground-based measurements of plasma velocity were made with this system in September 1972 (Taylor *et al* 1973) and multistatic observations continued until August 1975 when the availability of the site for the transmitter came to an end.

By taking full advantage of suitable aerials already in existence this IS system enabled a limited series of useful observations to be made at relatively low cost.

7.6. St Santin

When the French IS system was planned it also took advantage of an existing radio-telescope—the 40 m × 200 m reflector at Nancay. This telescope was designed in a novel way with the primary reflector steerable in elevation to provide a beam in the meridian. A transmitting aerial was therefore constructed due south of Nancay at a distance of 300 km (du Castel *et al* 1966). This was also of novel design; a parabolic section, 20×100 m^2, was mounted at an angle of 45° to the ground and illuminated by a horn feed via a secondary reflector, so that a CW beam with a frequency of 935 MHz was transmitted vertically upwards.

This bistatic system was very suitable for measuring plasma drift velocities along the field line. It also provided very good spectral detail with reasonable height resolution, features of the system that were especially important in the D and E regions.

There were, however, several limitations to the initial system. In order to examine different heights the 40×200 m^2 reflector had to be tilted and remain at each height until an adequate signal-to-noise ratio was obtained. For example, to sample the midday ionosphere at 15 separate heights between 100 and 500 km would take about an hour in all. Secondly, the bistatic system was unable to measure the plasma drift velocity in the plane perpendicular to the field line.

A full quadristatic system was therefore established by adding two more receivers at St Cassien and Mende (figure 27 (plate)). These sites were approximately 100 km west and east of the transmitter, and as they were much closer than the receiver at Nancay the antennae could be smaller in size without undue loss of signal-to-noise ratio. For each site 25 m parabolic dishes steerable in elevation were therefore chosen and both were fed by three primary horns mounted in a vertical plane so that three different heights can be observed simultaneously (Bauer *et al* 1974).

The overall design allows operation in several modes. By setting the three receiving antennae at three different elevations, seven different heights can be observed simultaneously. Alternatively, the two multi-beam antennae can be set to observe the same three heights continually, while the Nancay antenna can scan the range covered. This is a suitable procedure for measuring the total vector of plasma velocity at three different heights.

The French IS system is well suited for multistatic observations of plasma velocity at mid-latitudes and has made important contributions to the study of tidal movements of the neutral atmosphere and the measurement of electric fields associated with auroral disturbances (Testud *et al* 1975). It has also been able to contribute to a detailed study of the propagation of internal gravity waves; the profiles of N, T_e, T_i and V_p are observed above St Santin; the horizontal movement of ionospheric disturbances are monitored by Faraday rotation measurements in France and the

UK; and neutral-wind profiles are determined from incoherent-scatter, meteorological radar and normal meteorological measurements. Together, these data provide a picture of the propagation of atmospheric gravity waves and allow identification of the source of the waves (Bertin *et al* 1975).

7.7. Kharkov

Recently some information has been published about an IS installation in the USSR at the Kharkov Polytechnic Institute (Taran 1977). This is a monostatic two-channel system using a fixed parabolic antenna of diameter 100 m directed vertically upwards. Pulsed transmissions with peak powers of 2 MW can be used in single- or double-pulse modes, permitting height resolutions of 100 km or 10 km respectively. The use of two channels permits general flexibility in the system including Faraday rotation measurements. Measurements of electron density in the height range 150–1700 km and of T_i and T_e from 200–400 km have been carried out with this equipment.

8. Current developments

8.1. EISCAT

All the facilities listed in table 1 commenced observations in the decade 1962–72. The experience gained in using these has led to plans for a 'second generation' of IS facilities. One of these is already under construction in a joint project supported by six European countries (Federal Republic of Germany, Finland, France, Norway, Sweden and UK). Known by the acronym EISCAT (European Incoherent Scatter) this system will be located in North Scandinavia in the auroral zone.

Previous systems have been faced with the choice of using a high frequency to avoid coherent scattering by irregularities or a lower frequency to give the maximum height range for which $\lambda \gg D$. EISCAT will employ radars in both the UHF and VHF bands.

The UHF system will be tristatic with a transmitter located near Tromso in northern Norway and receivers at Tromso, Kiruna (Sweden) and Sodankyla (Finland) (figure 28). The transmitter will operate at 933·5 MHz, with a peak power of 2 MW. Each antenna will consist of a 32 m fully steerable parabolic dish.

The VHF system will be monostatic with both transmitter and receiver at Tromso. The operating frequency will be 224 MHz and the transmitter will provide a peak power of at least 5 MW. The main features of the EISCAT are summarised in table 2.

Both transmitters will have considerable flexibility in choosing a suitable waveform for each particular experiment. For example, to achieve a height resolution of 500 m pulse groups of variable spacing will be employed and each pulse within the group will be divided into subpulses according to a Barker code. In addition, it will be possible to change frequency between one pulse and the next, with a choice of 11 frequencies in all. This will avoid any ambiguity between the signals scattered at different heights from successive pulses. Finally, the VHF transmitter will be able to reverse the direction of circular polarisation from pulse to pulse.

The UHF system will measure a large number of parameters with high resolving power in the middle altitude range (100–500 km). It will be especially suitable for a study of the dynamics of the auroral atmosphere since the spaced receivers permit

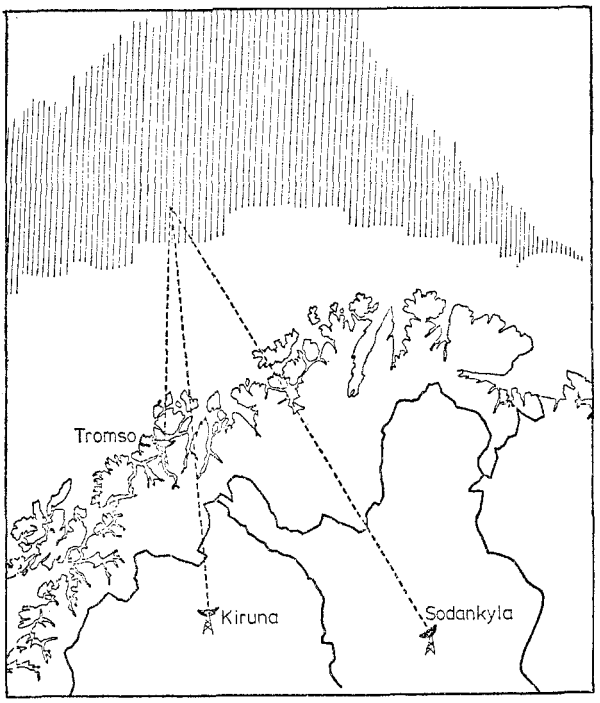

Figure 28. EISCAT stations. UHF system: 933 MHz transmitter at Tromso, receivers at Tromso, Kiruna and Sodankyla. VHF system: 224 MHz transmitter at Tromso, receiver at Tromso. Tromso–Sodankyla = 390·5 km, Tromso–Kiruna = 197·6 km, Kiruna–Sodankyla = 268·6 km.

measurements of the three velocity components of a single volume of moving plasma. Moreover, by steering the three antennae together so that they always observe the same volume at a given time, it will be possible to separate the spatial and temporal variations of the different parameters.

The VHF system will, among other things, extend the altitude range upwards

Table 2. EISCAT stations. *L* values at 300 km: Tromso 6·46, Kiruna 5·63, Sodankyla 5·25.

Station	Location	Magnetic dip	Antenna	Frequency (MHz)	Power Peak (MW)	Power Mean (MW)	Mode
Tromso	69·6° N 19·2° E	77·60	32 m parabola	933·5	2	0·25	Oblique, pulsed
Kiruna	67·9° N 20·4° E	76·77	32 m parabola	Receiving stations†			
Sodankyla	67·4° N 26·7° E	76·69	32 m parabola				
Tromso	69·6° N 19·2° E	77·60	Parabolic cylinder 120 m × 40 m	224	5	0·33	Oblique, pulsed

† The UHF (933·5 MHz) and VHF (224 MHz) transmissions will also be received at Tromso.

(~3000 km) and downwards (~80 km). The ability to radiate two orthogonally polarised signals will allow accurate electron density measurements to be made independent of the calibration of the transmitter and antenna. It is also hoped that the VHF system will be able to observe 'turbulent' scattering from heights of tens of kilometres (see §8.4 below) to probe the mesosphere and stratosphere.

For other measurements, the UHF and VHF systems are complementary. Thus the UHF system will be able to observe plasma lines near the peak of the F layer where $f_p > 6$ MHz while the VHF system will observe plasma lines over a wider range of altitudes, above and below the peaks, where 5 MHz $> f_p > 2$ MHz (see §4.1).

Also both the UHF and VHF systems will measure the ion–neutral collision frequency in the E region, but the optimum height for making this measurement at the two different frequencies is separated by about 20 km so that a greater height range will be covered than by a single system.

A facility as sophisticated as EISCAT, situated at high latitudes, is certain to make a major contribution to the study of solar–terrestrial physics in many different ways, and it is impossible to predict the full range of scientific investigations for which it will be used. The following list, however, gives some indication of experiments already planned.

(i) Ionospheric storms. Study of currents and particles which cause the atmospheric heating associated with magnetic storms. The resulting ion and neutral air velocities, and structural changes in the ionosphere and neutral atmosphere, will also be monitored.

(ii) Electric fields and currents. Measurement of plasma motion along and across magnetic-field lines and hence mapping of the electric fields generated in the magnetosphere by the solar wind. The system will also provide detailed data on the high-latitude current system.

(iii) Polar wind. The 'polar wind', i.e. the escape of light ions and electrons from the high-latitude atmosphere along magnetic-field lines, monitored up to heights of 2000 km or more.

(iv) Aurora. Auroral regions will be studied with a time scale of tens of seconds and a spatial resolution of about 1 km, and the system will also provide information on precipitating particles and their effects on the atmosphere. It may also be possible to study the wave–particle interactions involved in the precipitation of these particles.

(v) Atmospheric waves and tides. IS studies of atmospheric gravity waves suggest that many of these originate in auroral events at high latitude, and EISCAT will be able to study the generation of such waves. It will also complement the work carried out by IS facilities at lower latitudes on tidal motions in the upper atmosphere.

(vi) Atmospheric composition. Seasonal changes in both the D and F regions of the ionosphere are pronounced at high latitudes and are associated with changes of atmospheric composition. Data from the EISCAT facility should contribute greatly to understanding these phenomena.

It is expected that the EISCAT UHF system will begin observations in 1979 and that the VHF system will begin in 1980.

8.2. Ionospheric heating

Forty years ago Bailey (1938) discussed the strong absorption of energy by the ionosphere which occurs for frequencies near the electron gyro-frequency (~1 MHz)

and he concluded that with sufficient radiated power it should be possible to produce a significant artificial airglow in the ionosphere. Later he suggested that the local electron density would also be increased (Bailey 1959).

It is now well established that powerful MF and HF signals—not necessarily at the gyro-frequency—can significantly modify the ionosphere. The electron temperature near the level at which the signal is reflected can be raised and produce large changes in the ambient airglow. At the same time, recombination is reduced and so the electron density is increased.

Many of the effects of an HF signal, however, are not produced by simple ohmic heating. Thus large- and small-scale irregularities appear as artificial spread-F on an ionogram and give rise to scintillation effects in satellite or radio star signals propagating through them; these artificially induced irregularities may be due to a differential heating process, the precise nature of which is not determined. The small-scale irregularities (~ 3 m) are generated by parametric decay instabilities of plasma waves. Clearly the HF wave suffers an additional absorption of energy in creating an intense, turbulent spectrum of plasma waves. These plasma waves can accelerate electrons and so produce enhanced airglow emission through impact excitation of atomic oxygen.

IS systems are ideally suited to monitor the parameters of the upper atmosphere during the heating process, and also to make direct observations of the enhanced ion-acoustic and electron-acoustic waves. This has already been done at Arecibo where an HF transmitter is used to feed 100 kW at 5·62 MHz into the dish. Simultaneous use of the IS facility can monitor the increase in electron temperature due to normal deviative absorption, and by switching the heater on and off relaxation times (of a few tens of seconds) can be accurately measured for electron cooling. Powerful HF signals also increase the amplitude of the plasma lines. At Arecibo an enhancement of more than 10^4 has been observed, and this has been attributed to the decay mode of a parametric instability. The detailed spectra of the plasma lines strengthen this theory as the growing mode and the decay mode can be identified. The plasma lines themselves can of course be used to measure the plasma frequency (f_p) and hence the electron density. The decay time of the plasma lines in the daytime can be attributed to damping by photoelectrons and this has obvious applications in studying the flux of photoelectrons. The decay time at night is much slower, due to the absence of photoelectrons, and is primarily due to electron–ion collisions.

Here we have briefly listed some of the measurements that can be made when an IS facility is operated in conjunction with an HF heating experiment. It will be clear that the combination of an IS facility with HF heating experiments offer interesting possibilities and in association with the EISCAT project (mentioned in §8.1 above) the Max-Planck-Institut für Aeronomie is installing a high-power radio transmitter operating in the band 2·78–8 MHz for ionospheric modification experiments.

8.3. 'Coherent scatter'

The theory of 'incoherent' or 'thermal' scatter assumes that the average electron density is constant over a scale large compared with the wavelength of the probing signal so that only the random, thermally-induced ion-acoustic and electron-acoustic waves are observed. If, however, there are irregularities in the distribution of electron density corresponding to a wavelength Λ, these will give strong coherent back-scatter for a radar signal of wavelength 2Λ. Such irregularities exist throughout the iono-

sphere with characteristic correlation lengths ranging from several kilometres to a few metres. For signal wavelengths less than 1 m, however, it is generally found that coherent scatter from the ionosphere is not observed. Most IS facilities operate at wavelengths of 75 cm or less, but the Jicamarca radar uses a wavelength of 6 m. Moreover it lies near the magnetic equator and radiates signals vertically upwards: hence, it is especially sensitive to horizontally stratified or field-aligned irregularities with a vertical wavelength of 3 m. Thus the Jicamarca radar receives strong echoes from the regions of the equatorial electrojet (90 km to as high as 130 km) and during the night it also receives echoes from spread-F irregularities (Farley *et al* 1970, Fejer *et al* 1975). For observations in a direction exactly perpendicular to the magnetic-field line, such echoes can be up to 10^7–10^8 times as strong as the IS signal, so that even when the beam is offset by 3°, echoes received in the side-lobes of the array are still so strong that normal IS measurements are limited. Thus, electron density measurements are not normally possible below about 150 km, or for some F-region heights at night.

However, by recording the strong echoes, using specially modified RTI (range–time–intensity) equipment, useful results can be obtained (Woodman and La Hoz 1976). Apart from allowing the incidence of these irregularities to be monitored, the time delay of the strong echoes accurately defines their height while the Doppler shift of the return signal gives their velocity. Moreover, in the case of spread-F irregularities, normal IS measurements before and after the period when spread-F occurs, and even above and below the irregularities, can establish the background parameters of the ionosphere.

8.4. Mesospheric, stratospheric and tropospheric scatter

At Jicamarca scattered signals have also been detected from mesospheric (55–85 km) and stratospheric heights (10–35 km). The strengths of the signals from the 55–85 km levels vary considerably during the day and from one day to another. The signals are not observed at night. These mesospheric signals are generally consistent with those to be expected for incoherent scattering from D-region electrons but signal strengths 30 dB or more above noise level are sometimes observed. It is suggested that these stronger signals can be explained in terms of turbulent layers ($\sim$100 m thickness) in the mesosphere (Woodman and Giullen 1974, Rastogi and Woodman 1974). The theory of 'turbulent scattering' has been discussed by Rastogi and Bowhill (1976).

The strengths of the scattered signals from stratospheric levels are fairly constant throughout the day and night and show little variation from day to day. They are supposed to be due to dielectric fluctuations associated with clear air turbulence. By pointing the antenna a few degrees east and west of the zenith and measuring the Doppler shift of the echo signals horizontal and vertical wind components at both stratospheric and mesospheric levels have been measured.

Similar results have been observed at Arecibo and Chatanika, but here scattered signals have also been observed down to tropospheric levels. Figure 29(*a*) shows measurements at Arecibo of wind speed and direction over the height range 5–22 km together with independent measurements using balloons (rawinsondes). It will be seen that the two sets of measurements are in excellent agreement. Figure 29(*b*) shows similar measurements at Chatanika covering the height range 2–21 km.

This extension of the IS scatter technique down to the 5 km level represents

another remarkable advance and means that this technique can now provide continuous monitoring of a whole range of atmospheric parameters from a few kilometres to some thousands of kilometres.

8.5. Detection of the electron component

Until recently all IS measurements have been confined to those cases for which the radar wavelength (λ) is very much larger than the Debye length (D) in the iono-

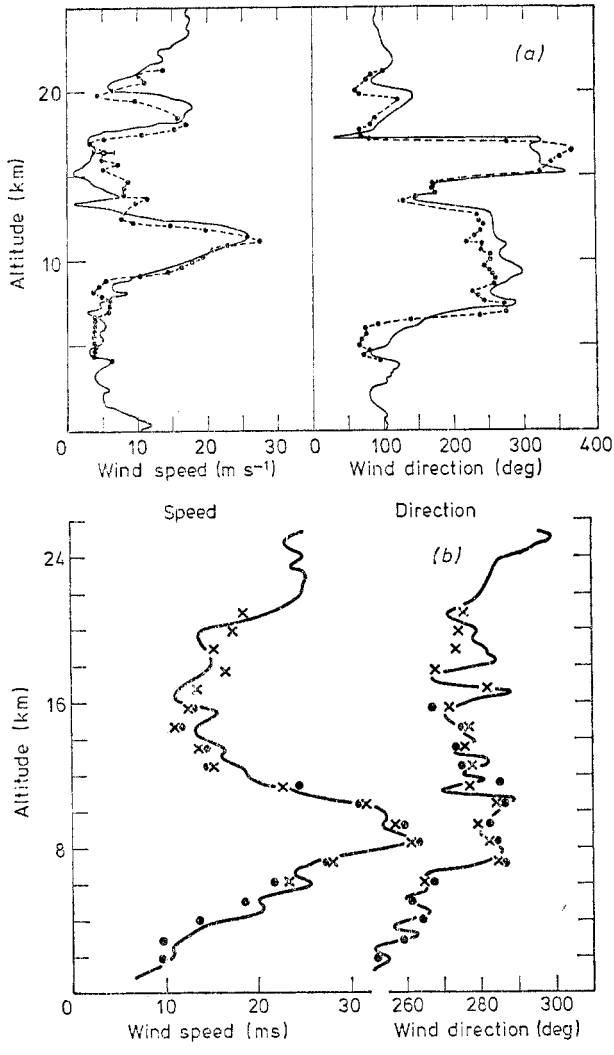

Figure 29. (*a*) Wind measurements at Arecibo, 6 April 1977, over height range 5–22 km, compared with sonde measurements (after B Balsley, private communication). — ● —, radar-derived winds, 19 h 39 m–20 h 13 m 60° W; ———, rawinsonde winds (San Juan), 19 h 00 m–20 h 51 m. (*b*) Wind measurements at Chatanika, 23 October 1976, over height range 2–21 km, compared with sonde measurements. ———, sonde, 1821 UT; ●, radar measurements, 1752 UT, 10 μs pulse; ×, radar measurements, 1834 UT, 10 μs pulse.

sphere. The main portion of the scattered power is then in the ion spectrum with the electron component concentrated in the two narrow plasma lines. As described in earlier sections of this review the detailed shape of the ion spectrum depends on T_e, T_i and m_i and it is this fact which has permitted these parameters to be measured accurately, especially under circumstances such as prevail at F-region heights for which a single ion species (O^+) dominates. At very great heights the Debye length increases to the extent that the assumption $\lambda \gg D$ is not valid, the electron component in the scattered radiation becomes relatively more important, and interpretation of the shape of the ion spectrum becomes more difficult because it then depends on a fourth parameter—electron density (N).

Recently, at the Arecibo Observatory, experimental confirmation of the transition from ion-dominated to electron-dominated spectra predicted by theory has been obtained (Hagen and Behnke 1976). To overcome the reduced signal-to-noise ratio for scattering at very great altitudes, long pulses of 5 ms duration were employed and this necessarily limited the height resolution. Furthermore, very long integration times (of several hours) were necessary. However, reliable results were obtained for four broad 1000 km height ranges centred near 850, 2000, 3000 and 4000 km. In the lowest height range only some 1% of the total scattered power was observed in the electron component whereas around the uppermost height range the proportion had increased to 90%. These experiments show that the IS technique can still yield valuable information on T_e and N, even in circumstances for which the usual criterion $\lambda \gg D$ does not apply and thus extends the applicability of the technique to plasmaspheric heights.

8.6. IS *from space vehicles*

Recently there has been some discussion of the possibility of IS measurements from space vehicles (Blanc *et al* 1976, Harker 1976). Of course the transmitter power and antennae dimensions available for such experiments aboard a satellite would be quite restricted, but short-range measurements might be possible. One potential advantage of using the technique on a space vehicle would be its ability to probe undisturbed regions around the satellite.

There are two serious constraints to such measurements. In the first place, reflections from the ground will swamp the return signal for all time delays in a range corresponding to reflection from directly below to reflection from the horizon of the vehicle. Thus a space vehicle radar at 300 km will be able to transmit and receive for a time interval of 2 ms, but then it would be saturated by ground clutter for a further 13 ms before transmission could resume. A second constraint follows from the movement of the satellite, so that integration of the scattered signal over a long period would correspond to averaging over a considerable horizontal distance. Harker (1976) has considered in some detail these factors for a space vehicle carrying a transmitter of mean power 4 kW and an antenna 10 m in diameter and concluded that with such a system ion-spectrum measurements would only be possible if averaged over a considerable horizontal distance, but that the plasma lines might be observed if they were enhanced by suprathermal electrons or by an HF signal. In future, satellites may well be equipped with much larger antennae, and capacitor banks could allow more powerful transmission for a limited time. With such developments, IS measurements from space vehicles may then be practicable.

Acknowledgment

In the preparation of this review the authors have drawn freely on published material and permission to reproduce the diagrams indicated is gratefully acknowledged.

References

Appleton E V and Barnett M A F 1925 *Proc. R. Soc.* A **109** 621–41
Bailey V A 1938 *Phil. Mag.* **26** 425–53
—— 1959 *J. Atmos. Terr. Phys.* **14** 299–324
Banks P M and Doupnik J R 1975 *J. Atmos. Terr. Phys.* **37** 951–72
Barker R H 1958 *Communication Theory* (London: Academic) p273
Bauer P, Cole K D and Lejeune G 1976 *Planet. Space Sci.* **24** 479–85
Bauer P, Lejeune G and Petit M 1970 *Planet. Space Sci.* **18** 1447–70
Bauer P, Waldteufel P and Vialle C 1974 *Radio Sci.* **9** 77–83
Bertin F, Testud J and Kersley L 1975 *Planet. Space Sci.* **23** 493–507
Beynon W J G 1974 *Contemp. Phys.* **15** 329–52
Blanc M, Bauer P and Lejeune G 1976 *Atmospheric Physics from Spacelab.* (Dordrecht: D Reidel)
Bowles K L 1958 *Phys. Res. Lett.* **1** 454–5
—— 1963 *Science* **139** 389–91
Booker H G and Smith E K 1970 *J. Atmos. Terr. Phys.* **32** 467–97
Breit G and Tuve M 1926 *Phys. Rev.* **28** 554–73
Buneman O 1962 *J. Geophys. Res.* **67** 2050–3
Carlson H C, Gordon W E and Showen R L 1972 *J. Geophys. Res.* **77** 1242–50
Carpenter L A and Kirchhoff V W J H 1974 *Radio Sci.* **9** 217–22
—— 1975 *J. Geophys. Res.* **80** 1810–4
Cicerone R J 1974 *Rev. Geophys. Space Res.* **12** 259–71
CIRA 1972 *COSPAR International Reference Atmosphere*
Cox L P and Evans J V 1970 *J. Geophys. Res.* **75** 6271–86
Dougherty J P and Farley D T 1960 *Proc. R. Soc.* A **259** 79–99
—— 1963 *J. Geophys. Res.* **66** 5473
du Castel F, Carru H, Petit M and Waldteufel P 1966 *Onde Elec.* **468** 281–4
Evans J V 1969 *Proc. IEEE* **57** 496–530
—— 1972 *J. Atmos. Terr. Phys.* **34** 175–209
—— 1974 *J. Atmos. Terr. Phys.* **36** 2183–243
Evans J V and Holt J M 1976 *Lincoln Laboratory, MIT Tech. Rep.* 522
Fabry C 1928 *C.R. Acad. Sci., Paris* **187** 777–81
Farley D T 1969 *Radio Sci.* **4** 935–53
—— 1970 *J. Atmos. Terr. Phys.* **32** 693–704
—— 1972 *Radio Sci.* **7** 661–6
Farley D T, Balsley B B, Woodman R F and McClure J P 1970 *J. Geophys. Res.* **75** 7199–216
Farley D T, McClure J P, Sterling D L and Green J L 1967 *J. Geophys. Res.* **72** 5837–51
Fejer J A 1960 *Can. J. Phys.* **38** 1114–33
Fejer B G, Farley D T, Balsley B B and Woodman R F 1975 *J. Geophys. Res.* **80** 1313–24
Gordon W E 1958 *Proc. IRE* **46** 1824–9
—— 1964 *Science* **146** 26–30
Gordon W E and Carlson H C 1974 *Radio Sci.* **9** 1041–7
Gray R W and Farley D T 1973 *Radio Sci.* **8** 123–31
Hagen J B and Behnke R A 1976 *J. Geophys. Res.* **81** 3441
Hagen J B and Hsu P You-Sen 1974 *J. Geophys. Res.* **79** 4269
Hagfors T 1961 *J. Geophys. Res.* **66** 1699–712
Harker K J 1976 *Radio Sci.* **11** 509
Hedin A E, Mayer H G, Spencer N W and Carignan G R 1974 *J. Geophys. Res.* **79** 215
Hey J S, Roberts J B G, Taylor G N and Watkins C D 1968 *Nature* **220** 865–8

Ioannidis G and Farley D T 1972 *Radio Sci.* **7** 763–6
—— 1974 *Radio Sci.* **9** 151–7
Jacchia L 1971 *Smithsonian Astrophys. Obs. Special Rep. No* 332
Leadabrand R L, Baron M J, Petriceks J and Bates H F 1972 *Radio Sci.* **7** 747–56
Moorcroft D R 1964 *J. Geophys. Res.* **69** 955–70
Petit M 1968 *Ann. Geophys.* **24** 1–38
Rastogi P K and Bowhill S A 1975 *J. Atmos. Terr. Phys.* **38** 399–411
Rastogi P K and Woodman R F 1974 *J. Atmos. Terr. Phys.* **36** 1217–31
Ratcliffe J A 1972 *An Introduction to the Ionosphere and Magnetosphere* (Cambridge: Cambridge University Press)
Salpeter E E 1960a *Phys. Rev.* **120** 1528–35
—— 1960b *J. Geophys. Res.* **65** 1851–2
Taran V I 1977 *Rad. Eng. Electron. Phys.* **21** 1
Taylor G N, Rishbeth H and Williams P J S 1973 *Nature* **242** 109–11
Testud J, Amayenc P and Blanc M 1975 *J. Atmos. Terr. Phys.* **37** 989–1009
Thomson J J 1906 *Conduction of Electricity through Gases* (Cambridge: Cambridge University Press) p321
Thuillier G, Falin J L and Wachtel C 1977 *J. Atmos. Terr. Phys.* **39** 399–414
Vidal-Madjar D, Kofman W and Lejeune G 1975 *Ann. Geophys.* **31** 227–34
Waldteufel P 1970 *Planet. Space Sci.* **18** 741–8
Wand R H 1970 *J. Geophys. Res.* **75** 829–38
Williams P J S and Taylor G N 1974 *Radio Sci.* **9** 85–8
Woodman R F and Guillen A 1974 *J. Atmos. Sci.* **31** 493–505
Woodman R F and La Hoz C 1976 *J. Geophys. Res.* **81** 5447–66
Yngvesson K O and Perkins F W 1968 *J. Geophys. Res.* **73** 97–110
Zamlutti C J and Farley D R 1975 *Radio Sci.* **10** 573–80

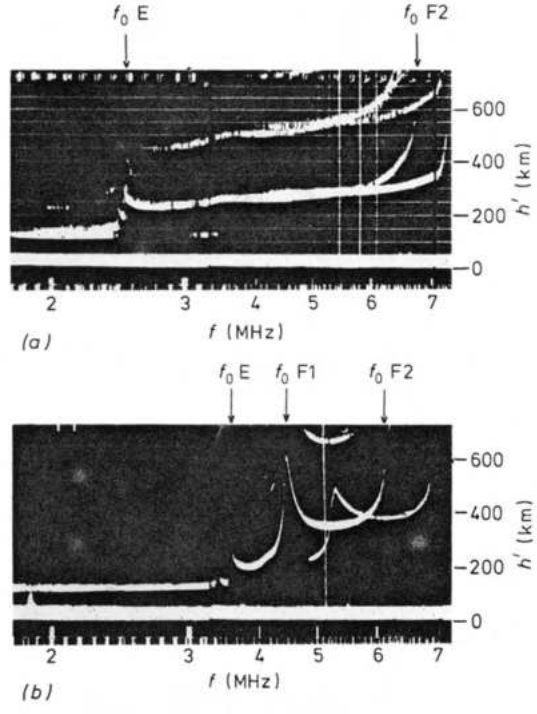

Figure 1. Daytime ionograms for a mid-latitude station (*a*) in winter, (*b*) in summer, showing critical frequencies, ordinary and extraordinary traces and multiple reflections.

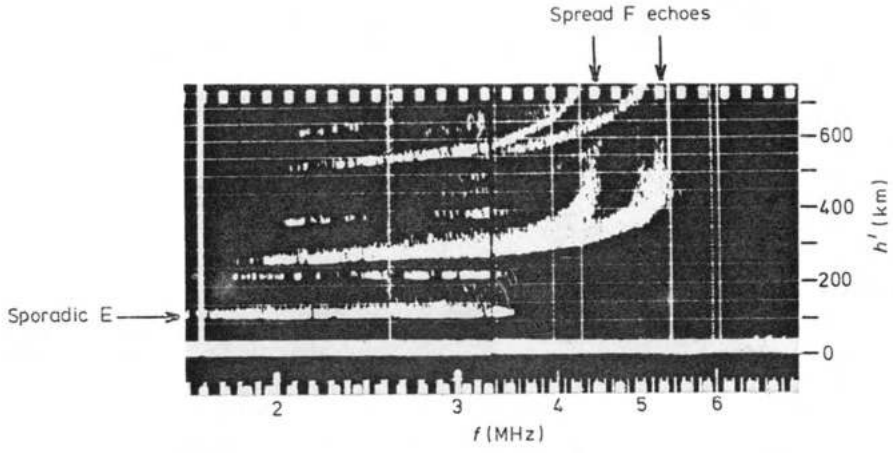

Figure 3. Sporadic-E and spread-F echoes.

see page 912

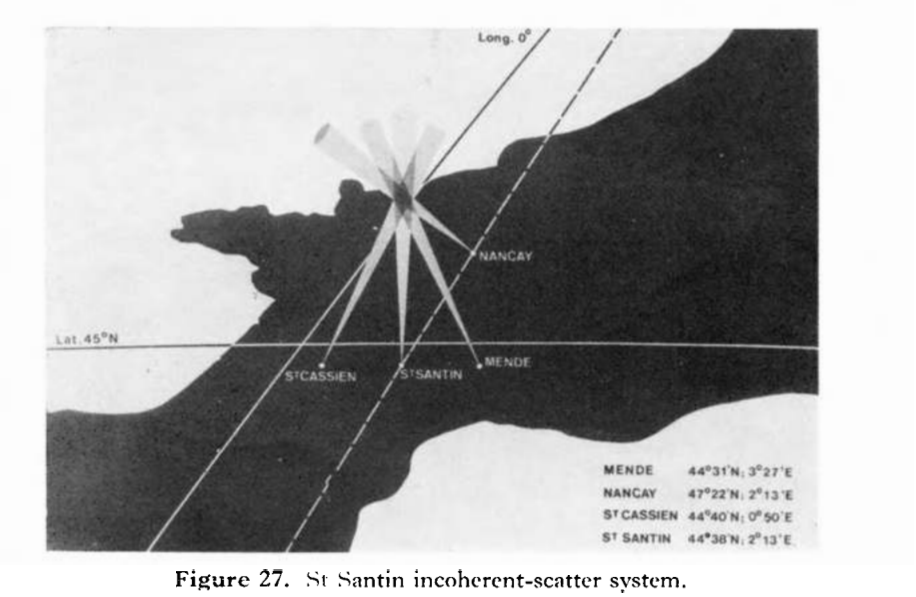

Figure 27. St Santin incoherent-scatter system.

see page 947